NOTE TO USERS

This reproduction is the best copy available.

Fabrication of AlN-MgO-MgAl$_2$O$_4$ Ceramic Composite by Spontaneous Reactive Infiltration

HESAM NASERY

A Thesis

in

The Department

of

Mechanical and Industrial Engineering

Presented in Partial Fulfillment of the Requirements
for the Degree of Master of Applied Science (Mechanical Engineering) at
Concordia University
Montreal, Quebec, Canada.

April, 2008

Library and
Archives Canada

Published Heritage
Branch

395 Wellington Street
Ottawa ON K1A 0N4
Canada

Bibliothèque et
Archives Canada

Direction du
Patrimoine de l'édition

395, rue Wellington
Ottawa ON K1A 0N4
Canada

Canada

ABSTRACT

Fabrication of AlN-MgO-MgAl$_2$O$_4$ Ceramic Composite by Spontaneous Reactive Infiltration

Hesam Nasery

Aluminum nitride ceramics are in high demand in electronic industries as substrate materials for applications requiring high thermal conductivity. Sintering and hot pressing are the most common processing methods used to make dense AlN ceramics. However, all methods of AlN sintering involve high temperatures and long times. Therefore, it is an expensive material. Removing oxygen, as a main impurity of aluminum nitride, by a low cost method in order to achieve dense and high thermal conductivity aluminum nitride ceramics has been pursued for many years.

A pressureless infiltration technique at low (650-950°C) temperature was developed to fabricate aluminum nitride-based ceramic matrix composites. The process involves forming a particulate porous compact of non-sintered aluminum nitride and introducing magnesium alloy into the channel network by spontaneous infiltration in a nitrogen atmosphere. Magnesium oxide and spinel phase (MgAl$_2$O$_4$) were formed in-situ, when nitrogen gas was used. Densification, thermal properties, and microstructure of the products have been studied. Microstructural, phase, and chemical analysis show that AlN-MgO-MgAl$_2$O$_4$ ceramic composites can be fabricated successfully. Metallic phases were not observed in the samples fabricated at higher than 800 °C and electrical conductivity results show that they are insulators. Thermal diffusivity and heat capacity have been measured using nano-flash and differential scanning calorimetry techniques,

respectively. Thermal conductivity results are strongly influenced by the residual porosity. Maximum thermal conductivity and density at room temperature were measured to be 95.88 W/m.K and 2.451 g/cm³, respectively.

ACKNOWLEDGEMENT

To my father and mother…..

TABLE OF CONTENTS

LIST OF FIGURES

LIST OF TABLES

NOMENCLATURE

CTE	Coefficient of Thermal Expansion
C_p	Heat Capacity (J/g°C)
G	Gibbs Energy of the System under Consideration (KJ/mol)
H	Enthalpy (W/g)
K	Thermal Conductivity (W/mK)
Q	Heat Flux per Unit Time per Unit Area (W)
R	Electrical Resistivity (Ω.cm)
t	Holding Time (min)
T	Temperature (°C)
D	Thermal Diffusivity (mm²/S)
XRD	X-Ray Diffraction

Greek Letters

α	Contact Angle in Equation 2.9 (Degree)
θ	Diffraction Angle (Degree)
ε	Porosity
ν	Velocity of Carrier (mm/s)
λ	Mean Free Path (mm)
γ	Surface Tension Energy (J)
η	Viscosity (Pa.s)
ρ	Density (g/cm³)

CHAPTER 1: INTRODUCTION

In recent years, the electronic industries have experienced significant improvements. When the first transistor was invented in 1959, electronic chips could hold a single circuit element. Nowadays, millions of elements such as transistors, capacitors, and resistors have been mounted onto a single ceramic chip such as silicon carbide or aluminum nitride as electronic substrates. In order to ensure reliability and efficiency of electronic devices made of these elements, management of thermal dissipation and thermal expansion matching in electronic substrates is required. The issues of thermal conductivity, coefficient of thermal expansion, density, electrical resistivity, mechanical strength, chemical stability, environmental compatibility, and cost of material substrates have been considered by industries [1,2].

Aluminum nitride and its composites are often cited as a potential substrate material for future electronic industries due to some unique properties such as high thermal conductivity and low dielectric constant [3]. This study aims at the low temperature fabrication of non-sintered AlN-based composites by spontaneous infiltration with AZ91E, magnesium alloy.

Although aluminum nitride is not a new ceramic (synthesized in 1877), it was not used until its potential in the thermomechanical and high performance electronic industry was realized (mid 1980s) [4]. It has attracted much attention over the past few decades by electronic industries due to the following properties:

- Low dielectric constant

- High electrical resistivity

- Good mechanical properties

- Coefficient of thermal expansion close that of silicon

- High thermal conductivity

- Non-toxicity

Interest in aluminum nitride has increased after Borom et al. [5] clarified that AlN is a good phonon heat conductor. Later, Slack et al. [6,7] studied the thermal conductivity of many nonmetallic crystalline and single crystal materials, including AlN, and predicted high thermal conductivity (~320 W/m.K) of single crystal aluminum nitride. Nipko et al. [8] revealed that AlN has the capability of operating in electrical devices at elevated temperatures. The idea behind using high thermal conductivity substrates is due to dissipation of heat through the substrate material with the advantage of not using external cooling facilities. Therefore, the demand for high thermal conductivity materials to develop high density integrated packages has increased [9,10].

The thermal conductivity of AlN is at least 5 to 8 times larger than that of alumina and close to that of silicon carbide, the current materials used for substrates. Alumina (Al_2O_3) has low thermal conductivity (~20 W/m.K) and a high coefficient of thermal expansion (7.2×10^{-6} /°C) compared to that of silicon carbide (3.2×10^{-6}/°C) and it is not suitable for the requirements of advanced integrated circuit applications. Miyashiro et al. [9] recommended that AlN can replace alumina due to its high thermal conductivity. A wide range of thermal conductivities for crystalline AlN has been reported from 50W/mK to 270 W/m.K. However, the reasons for such discrepancies are not obvious [4,11]. The most important obstacle for commercializing aluminum nitride apart from cost, is the

2

lack of reproducibility in thermal conductivity and the adhesion of metallization layers [12,13]. Aluminum nitride powder is synthesized by various methods such as carbothermal reduction, direct nitridation, floating nitridation, and chemical vapor deposition [14,3]. In addition, AlN has been used in electro-optics fields and structural applications such as crucibles [14].

With the advent of composites, ceramics play a drastic role in composite structures. The need for high performance and lightweight materials has persuaded researchers to develop magnesium composites with cost effective fabrication technologies. Magnesium alloys have some unique properties such as excellent castability, superior machinability, and high specific strength. Furthermore, they are one of the lightest materials known in engineering applications. Those properties have encouraged researchers to use magnesium matrix composites for some demanding applications [15]. Conventionally, magnesium matrix composites have been fabricated with different ceramic particles as reinforcing phases such as SiC, TiC, and AlN, through stir casting [16], squeeze casting [17], or powder metallurgy [18]. An increased tensile strength up to 237 MPa with 2.04 g/cm^3 density for magnesium metal matrix composites reinforced with alumina short fibers by squeeze casting method has been reported [19,20]. Among traditional approaches to produce such composites, spontaneous infiltration has been used as a low cost and near-net shape method. Leon et al.[21] reported fabricating Mg/AlN composite using an infiltration technique with a linear coefficient expansion (CTE) of 7.65×10^{-6} /°C, which is higher that of AlN (4.4×10^{-6}/°C) and lower that of magnesium (24×10^{-6}/°C) [21,22].

3

The aim of this work is to study magnesium infiltration into a non-sintered AlN preform at relatively low temperatures (650-950°C) to achieve a dense AlN composite with appropriate thermal properties comparable to that of sintered aluminum nitride ceramic. It focuses on spontaneous liquid infiltration of molten magnesium alloy into porous AlN using in-situ reaction in a nitrogen atmosphere.

Chapter 2 briefly outlines AlN properties and fabrication processes of magnesium matrix and AlN matrix composites and gives objectives of the present work. Methodology and experimental setting are given in Chapter 3. In Chapter 4, all theoretical and experimental results including microstructural, phase and chemical analyses, thermal properties, electrical resistivity, and density measurements will be discussed. Conclusions, contributions, and recommendations for future work are given in Chapter 5. Appendix A presents the method of thermal diffusivity measurement. In Appendix B, the results of all calculation related to heat capacity are reported. Crystallographic data of products and reactants are presented in Appendix C.

CHAPTER 2: LITERATURE REVIEW

Ceramics are inorganic materials that can be defined as compounds between metallic and non-metallic elements. They have been used by mankind for many thousands of years. Up to the 1950s, the most important ceramics were termed traditional ceramics such as pottery, bricks, clay, and porcelain. More recently, ceramic materials are playing a significant role in industrial applications involving the research and development of electronic systems. In the twentieth century, important progress has been made in understanding the unique properties of these materials such as electrical insulation, mechanical strength, and thermal stability. Eventually, a new class of these materials with high performance, including oxide and non-oxide materials for technical applications, has emerged and has been termed engineering or advanced ceramics [23-26].

2.1 Aluminum Nitride

2.1.1 Crystal Structure of AlN

Aluminum nitride has a strong covalent nature (60% covalent, 40 % ionic), and crystallizes with a hexagonal structure under the Wurtzite[1] type $a = 3.111$ nm and $c = 4.978$ nm. In the AlN unit cell, aluminum atoms fill tetrahedral sites half-occupied by nitrogen atoms (Fig 2.1) [14,27,28].

Reduction of the c lattice parameter has been correlated to higher oxygen concentration and lower thermal conductivity of the AlN grains by Baranda et al. [29].

---

[1] Wurtzite is a mineral crystal form of zinc sulfide, named after French chemist Charles-Adolphe Wutz.

Introduced Al vacancies result in a decrease in the *c* lattice parameter and increased phonon scattering defects. Oxygen in synthesized AlN forms a spinel phase which reduces the thermal conductivity. Minor additions of oxygen to AlN result in a variety of structures based on either AlN or spinel.

In the Al-N system, aluminum nitride with the hexagonal wurtzite crystal structure is the only stable phase at ambient pressure.
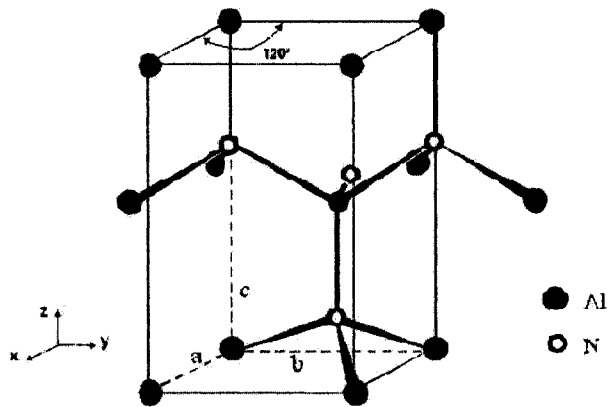
Figure 2.1: *The crystal structure of AlN [27]*

2.1.2 Aluminum Nitride Properties

The thermal property of AlN along with electrical and mechanical properties of AlN will be discussed in this section.

2.1.2.1 Thermal Conductivity

Thermal conductivity is an intrinsic property of each material that indicates the ability for transferring heat. It is a critical property for any ceramic used as an electronic substrate material [30]. Thermal conductivity is defined by the Fourier equation [31]:

$$\frac{dQ}{dt} = -KA \frac{dT}{dX} \qquad\qquad \textbf{2.1}$$

Where dQ is the quantity of heat transmitted normal to the area A during time dt through thickness dX due to temperature difference dT. K is the thermal conductivity which has units of W/m.K. The minus sign indicates that the heat always flows from hot to cold regions. The amount of heat transfer is controlled by the:

- Amount of heat energy present

- Nature of heat carrier in the material

- Amount of heat dissipation

The heat energy present is a function of the volumetric heat capacity. The carriers are electrons and phonons (lattice vibration waves). The amount of heat dissipation depends on the average distance covered by lattice waves, or mean free path. The thermal conductivity, K, is directly proportional to the heat capacity c, the quantity and velocity of the carrier v, and the mean free path λ:

$$K \propto c \upsilon \lambda \qquad\qquad \textbf{2.2}$$

In metals, heat is carried by free electrons (K_e) which are relatively free to move throughout the structure due to the metallic bonding. Thermal conductivity in pure metals is high because of a huge number of carriers and long mean free path. On the other hand, alloys have lower thermal conductivity rather than pure metals due to a reduction of mean free path. In nonmetallic materials, heat is carried by phonons (K_l) and radiation at high temperature (K_r). Hence, total thermal conductivity is given by [14,23,26,28]:

$$K = K_l + K_e + K_r \qquad\qquad \textbf{2.3}$$

Impurities, porosity, micro-cracks, grain boundaries, grain size, and secondary dispersed phases are some factors which affect thermal conductivity of ceramics. Among these factors, porosity has a dramatic influence on thermal conductivity. Under most circumstances, increasing pore volume will result in a reduction of thermal conductivity. It is because of the slow heat transfer across pores [14,23,28]. In a crystalline ceramic material, the basic requisites for high thermal conductivity are [4,14]:

- Low atomic mass

- Strong interatomic bonding

- Simple crystal structure

- Low anharmonicity

- High purity

These properties are best fulfilled with diamond. In 1911, Eucken [32] realized that diamond is a superior conductor for heat at room temperature. This idea was theoretically supported by Debye in 1914 [33]. Berman et al. [34] reported a thermal conductivity for diamond of 2000 W/m.K at room temperature. Beside diamond, boron nitride also has a high thermal conductivity at room temperature. However, they are both expensive and their manufacturing process has not yet been optimized. Beryllium oxide (BeO) is another material with high thermal conductivity, but it is not being used any longer because it is toxic [9]. Therefore, aluminum nitride is considered a promising substrate material for integrated circuits (IC). As mentioned earlier, the theoretical thermal conductivity of single crystal AlN is estimated to be 320 W/m.K [8,9]. The thermal conductivity of AlN ceramics is severely influenced by its chemical purity and

8

density. There have been several reports published on thermal conductivity of AlN ceramics, which range from 10 to 272 W/mK due to the presence of impurities and porosity [6,35,36]. Oxygen has been found as the most important impurity. Dissolved oxygen ions, either from incomplete conversion of Al_2O_3 or crude processing of AlN, occupy nitrogen sites in the AlN and generate Al vacancies to compensate for the electric charge [27,37]. Full densification of AlN is difficult due to its high covalent bonding and these oxygen impurities. Various parameters such as sintering conditions, holding temperature, holding time, and the quantity of sintering additives have been studied in order to make high thermal conductivity and dense, AlN [37]. The highest value of thermal conductivity for polycrystalline AlN has been reported by Nakano et al.; 272 W/m.K for AlN sintered at 1900 °C for 100 hours under nitrogen gas [36]. Table 2.1 shows summarises values of AlN thermal conductivity. Results show that the sintering process involves high temperature and long times.

Table 2.1: *Thermal conductivity of aluminum nitride*

Reference	Thermal Conductivity of AlN at room Temperature (W/m.K)	Additives	Remark
Y. Baik [14]	160-270	Y_2O_3	Sintering at 1750°C - 1950°C (1 h.)
H. Nakao et al. [36]	272	Y_2O_3	Sintering at 1900°C (100 h.) under Nitrogen atmosphere
Y. Kurokawa et al. [38]	160	No additives	Hot pressing at 1800°C
T. Okada et al. [39]	155	Y_2O_3	Hot pressing at 1900°C
Kasori et al. [37]	245	Y_2O_3	Sintering at 1850°C (30 min.) and annealing at 1850°C (100 h.)
Baranda et al. [29,40]	114-194	SiO_2 and Y_2O_3 CaO	Sintering at 1825-1860°C (1 h.)
Kuramoto et al. [11]	175	$CaO.Al_2O_3$	Sintering at 1800°C (1h.) under Nitrogen atmosphere
Watari et al. [50]	180	Y_2O_3	Sintering 1500°C to 1900°C (1h.)

2.1.2.2 Physical and Chemical Properties

The color of the AlN crystal varies from white to various shade of blue. Generally, pure aluminum nitride is white, and the blue one is by reason of the presence of about 7% aluminum oxycarbide, Al_2OC, which resulted from reaction between aluminum and carbon monoxide during the carbothermal reduction synthesis method [41]. The most important physical and mechanical properties of AlN compared with those of BeO, Al_2O_3, and SiC, are shown in Table 2.2. Mechanical properties of AlN substrate show that it is more machinable than Al_2O_3 [37].

The melting point or decomposition temperature of AlN has been reported at 2800°C under a nitrogen pressure of 10 MPa [42].

Due to the significance of the surface condition on sintered properties, several studies have been focused on aluminum nitride powder oxidation. Aluminum nitride powders have good resistance to oxidation in air at room temperature. Therefore, no oxidation takes place below 700-750°C in air without moisture. Oxidation of AlN powder starts between 750-1100°C with the formation of the corundum phase (α- Al_2O_3) [43,44,45]. The oxidation process depends on particle size, temperature, and humidity of the environment. The oxidation of AlN proceeds based on the following equation [14,46]:

$$4AlN + 3O_2 \rightarrow 2Al_2O_3 + 2N_2 \qquad\qquad \textbf{2.4}$$
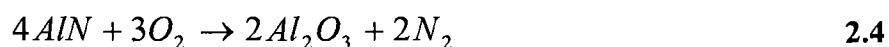
Table 2.2: *Physical and mechanical properties of ceramics used for substrates*

Properties	AlN	Al₂O₃	BeO	SiC	References
Density (g/cm³)	3.25	3.89	2.90	3.217	[12,23,25]
Flexure strength (MPa)	340-490	304-314	245	---	[12,14,26,35]
Vickers hardness (GPa)	11-12	23-27	12	24	[4,15,34]
Bulk modulus (GPa)	202-237	--	--	--	[26]
Light transmission (%) (λ= 6μm, t= 0.5 mm)	48	opaque	opaque	----	[35]

On the other hand, Slack et al. [42] reported that in the presence of moisture, a surface oxidation rate between 5 to 10 nm of oxide per day at room temperature takes place according to the following equation:

$$AlN + 2H_2O(g) \rightarrow AlO \cdot OH + NH_3 \quad \underline{\textit{Low Temperature hydrolysis} < 100\ ^{\circ}C} \quad \textbf{2.5}$$
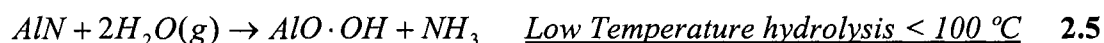
Whereas, Abid et al. stated this reaction does not take place readily with atmospheric moisture at room temperature [43]. Another hydrolysis reaction between 100°C and 300°C has been reported as follows [46]:

$$2AlN + 3H_2O(g) \rightarrow Al_2O_3 + 2NH_3 \quad \underline{High\ Temperature\ hydrolysis\ (100\text{-}300\ ^\circ C)} \quad \textbf{2.6}$$
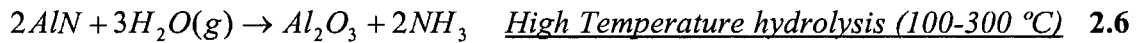
The oxidation rate of aluminum nitride is slow even at high temperature due to the formation of a dense, adherent aluminum oxide film on the surface.

2.1.2.3 Electrical Properties

Electrical properties of AlN, such as electrical resistivity, dielectric constant, dielectric strength, and breakdown voltage are also fascinating for electronic industries. Table 2.3 summarizes the electrical properties of AlN and other materials. For general use, materials with electrical resistivity more than 10^{10} Ω-cm are classified as good electrical insulators [47]. Figure 2.2 shows the range of electrical resistance of conductors, semiconductors, and insulators.

Low Resistivity type   Medium Resistivity type

| Conductor | Semiconductor | Insulator |

10^{-5} 10^{0} 10^{5} 10^{10} 10^{15}
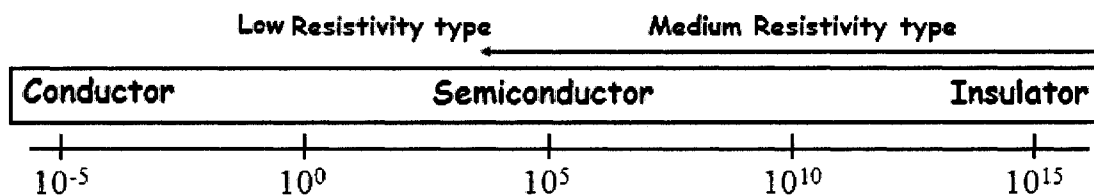
Figure 2.2: *Electrical resistance range (Adapted from [47])*

Table 2.3: *Electrical properties of AlN and some ceramic used as substrates [9,26,37]*

Item	unit	AlN	Al_2O_3	BeO	SiC
Volume resistivity	Ω-cm	$>10^{14}$ Insulator	$>10^{14}$ Insulator	$>10^{14}$ Insulator	$>10^{14}$ Insulator
Dielectric Strength	kV/cm (25°C)	140-170	100	100	0.7
Dielectric constant	1 MHz (25°C)	8.9	8.5	6.5	40

2.1.3 Sintering Mechanism of AlN

In general, a process for forming a denser mass by heating (at 0.4-0.5 T_m (k)) compacted powder is technically termed as sintering. The sintering process usually results in removal of pores and strong bonding between adjacent particles [14,24]. AlN has poor sinterability due to low self-diffusivity [10,14,26]. Therefore, to enhance sinterability, sintering aids such as rare earth compounds (Y_2O_3, YF_3, $Y_3Al_{15}O_{12}$), alkaline earth compounds (CaO, $CaCO_3$), or other compounds (MgO, TiO_2, etc.) are used [48]. An appropriate additive for sintering AlN has to have the following characteristics [14,49]:

1- Chemical compatibility with aluminum nitride

2- High electrical resistivity in order to prevent electrical short circuits

3- Formation of liquid phase at the sintering temperature (around 2000K)

Among the many sintering additives, Y_2O_3 meets almost all above requirements and the use of Y_2O_3 results in high thermal conductivities. Watari et al.[50] observed that adding 1 mol% of Y_2O_3 can increase the thermal conductivity of aluminum nitride to 180

W/mK for sintering at 1500 to 1900°C for 1 hour (Table 2.1). Besides yttria alone, many studies [11,39,40,51] on the use of combinations of Y_2O_3 and other additives such as CaO and SiO_2 have been reported. During sintering, aluminum vacancies in the AlN lattice which have been created by incorporating oxygen on the nitrogen sites (by substitutional solution) cause a phonon-defect scattering. The resulting mass difference of the occupied Al sites and the aluminum vacancies generates lattice anharmonicity in AlN. A key defect which limits the thermal conductivity of AlN are the vacancies associated with the soluble oxygen [47,48]. Available commercial AlN powders have around 1 wt% of oxygen as a surface layer of oxide or aluminum oxy-nitride. The role of the additives is to form a liquid phase by reaction with surface Al_2O_3 and to act as an oxygen getter to remove oxygen from the AlN lattice [9,14,26]. The sintering aids react with the aluminum oxide surface layer at sintering temperature to make a liquid phase (liquid phase sintering). Consequently, alumina and yttria form three types of Y-Al-O compounds in the triple point of the grain boundaries [12,14,26]. Finally, to remove oxygen entirely from the AlN ceramics a new method was tried by Shinzoke et al.[54] and Nakano et al. [35]. In this method, they found that a reducing atmosphere such as carbon monoxide with nitrogen changed the aluminum oxides to aluminum nitrides and carbon monoxide to carbon dioxide. However, the reactions and the mechanisms which enhance the thermal conductivity under a reducing gas are not quite clear yet. The possible reactions taking place during sintering of aluminum nitride with Y_2O_3 in a CO reducing gas are [50]:

$$Al_2O_3 + N_2 + 3CO \rightarrow 2AlN + 3CO_2 \qquad \textbf{2.7}$$

$$2Y_2O_3 \cdot Al_2O_3 + N_2 + 3CO \rightarrow 2AlN + 2Y_2O_3 + 3CO_2 \qquad \textbf{2.8}$$

$$Y_2O_3 + N_2 + 3CO \rightarrow 2YN + 3CO_2 \qquad \underline{at >1850\ ^\circ C} \qquad \textbf{2.9}$$

Sintering Mechanism for High Thermal Conductivity AlN
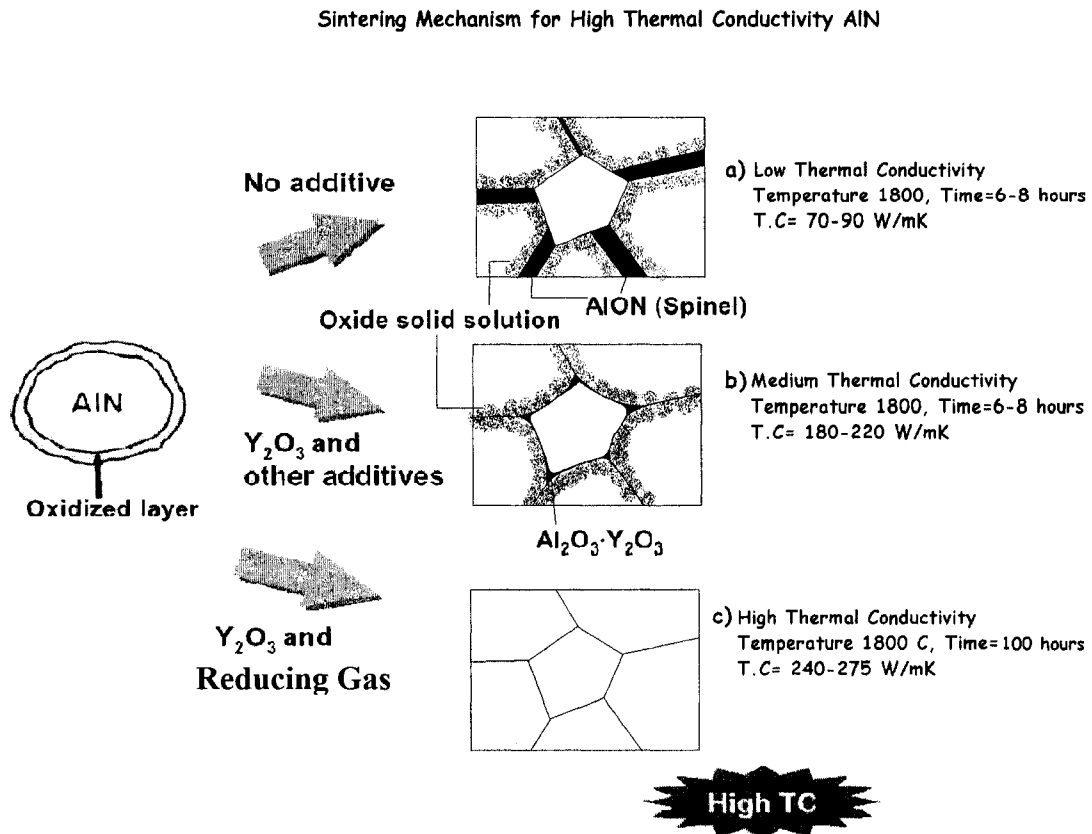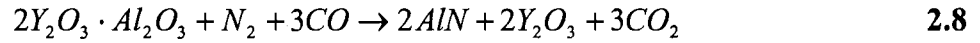
Figure 2.3: *Sintering mechanism of Aluminum nitride [9,55]: (a) No additive case: oxygen remains in spinel layers and oxygen solid solution. (b) Yttria as an additive: oxygen remains in triple points (c) Yttria and reducing Nitrogen gas: oxygen was almost eliminated*

Figure 2.3 shows a schematic of AlN sintering following three routes. The sintering process of AlN can be performed in the vapor-phase, solid phase, liquid phase, and reactive phase sintering which are based on the material transport mechanism [10,27].

The highest value thermal conductivity reported is 272 W/m.K for AlN sintered at 1900°C for 100 hours under reducing nitrogen gas [36].

2.2 Fabrication of Magnesium/Aluminum Nitride Composites

Mg/AlN composites have been introduced as a novel metal matrix composite by Arroy et al. [22]. They studied mechanical properties and the infiltration process of molten magnesium into sintered AlN preforms under argon atmosphere at 950°C. In addition, fabrication of AlN composites in some systems such as Mg/AlN,MgO [21], Mg/AlN,MgAl$_2$O$_4$ [22], AlN/MgO [56], or AlN/Al$_2$O$_3$,MgO [57] have been reported. However, fabricating AlN/MgO,MgAl$_2$O$_4$ composites at low temperatures (<1000 °C) with reactive infiltration of molten magnesium into non-sintered AlN powder in order to achieve high thermal conductivity could not be found in the literature. The present chapter highlights the relevant processing techniques to fabricate Mg-matrix and AlN-matrix composites.

In general, the combination of two or more engineering materials (Metals, Polymers, Ceramics) to produce a new material, whose properties are designed to be superior to those of the constituent materials, is called a composite. In the middle of the nineteenth century, wooden planking with iron frames as a composite material was used in construction industries. The modern composites have been developed in the aircraft industry in the middle of the twentieth century [58].

2.2.1 Processing of Magnesium Matrix Composites

Generally, metal matrix composites consist of a metallic matrix combined with a ceramic (Oxides, Carbides) as a reinforcing phase. Magnesium, because of some specific properties such as low density, high specific strength, and availability, is receiving attention by many industries. Distributing the reinforcing phase in the matrix in a homogeneous way is the key challenge in the processing of magnesium matrix composites [3,23]. Fabrication of magnesium matrix composites reinforced with some ceramics such as AlN, MgO, SiC, and TiC can be classified into two categories as liquid state and solid state techniques. Stir casting, infiltration, spray forming, and in-situ processing are some examples of liquid state processing. Most metal matrix composites are produced through liquid state processing methods, due to the ability of the liquid metal to take any complex shape. Molten metal incorporates the dispersed phase, followed by solidification. In these techniques, high mechanical properties can be obtained by proper interfacial bonding (wetting) between molten the metal and dispersed phase [3,60].

2.2.1.1 Stir Casting

In this method, the reinforcing phase is distributed into the molten metal by mechanical stirring. Low cost, high productivity, and near net shape capability makes the stir casting method a good technique for mass production [16,61]. Magnesium composites with various matrix compositions have been reported by stir casting [62,63]. Ray used this method to fabricate Al/AlN(p) composites [64]. Figure 2.4 illustrates a typical stir casting process of magnesium matrix composites. Due to the different densities of SiC particles

(3.2 g/cm³) and magnesium (1.74 g/cm³), the particles will deposit unless the melt is agitated.
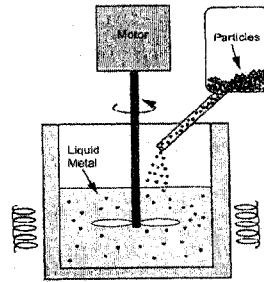
Figure 2.4: *Stirring of composite melt with ceramic particles to minimized settling of the particles during processing [3]*

2.2.1.2 Infiltration

In this technique, preformed[1] reinforcing phase (ceramic particles, fibers, etc...) is immersed into the molten matrix metal. The space between two particles is filled by molten metal. The driving force for this technique is either capillary force (spontaneous infiltration), or an external force (vacuum or pressure infiltration) [3]. In pressure-driven infiltration, the molten metal is forced into a ceramic preform by hydraulic or mechanical means. Typical pressures are between 1 and 20 MPa depending on the extent of wetting of the ceramic by the molten metal [3,65,66]. Apart from cost of the equipment and tooling, deformation and breakage of the preform during pressure application are major problems in the pressure infiltration method [60,66].

Squeeze casting is a pressure infiltration method. A movable part for applying pressure is placed on the molten metal and forces it to penetrate into the preform (Figure 2-5).

---

[1] The preform is an agglomerate or a compact of the reinforcement, which may be in the form of particles, whiskers or fibers.

18
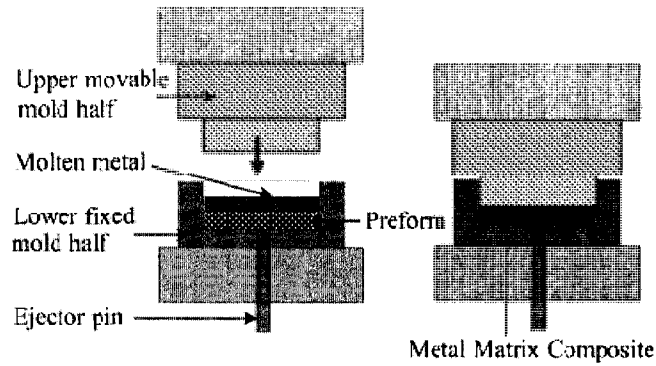
Figure 2.5: *Schematic of squeeze casting process [59]*

Magnesium matrix composites such as Mg/SiC_w and AZ91/SiC_w, have been produced using this technology, however, the amount of pressure has to be controlled properly [67,68]. Excessive high pressure produces a turbulent flow of molten magnesium. This causes gas entrapment and magnesium oxidation, which affects the microstructures and mechanical properties of the composites [60]. A two step squeeze casting process (indirect squeeze casting), consisting of infiltration at low pressure and solidification at high pressure has been introduced to fabricate ZK51A/SiC_w composites by Hu et al. [69].

In vacuum-driven infiltration, the driving force for infiltration is the applied vacuum [70,71]. In spontaneous infiltration, molten metal can be drawn through the channels of the porous preform simply by capillarity. The molten metal wets the skeleton of the porous ceramic. Aghajanian et al. [72,73] introduced this method to fabricate Al/Al_2O_3 and Al/SiC composites under nitrogen atmosphere. Kaneda et al. [74] fabricated a Mg/SiC composite by this method. A schematic set-up of spontaneous infiltration is shown in Fig 2.6.

19
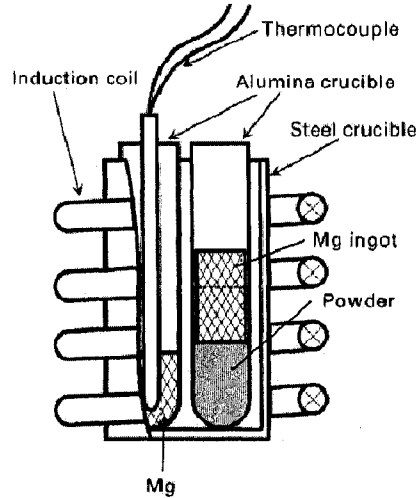
Figure 2.6: *Experimental setup for spontaneous infiltration [60]*

Leon et al. fabricated a Mg/AlN composite using infiltration of molten magnesium into sintered AlN at 870-960°C under argon atmosphere [21]. They achieved 90-110 GPa elastic modulus and 70-80 HRB hardness. Furthermore, a linear coefficient of thermal expansion of 7.65×10^{-6} /°C, in the temperature range of 215-315°C was reported which is lower than that of Al/AlN composites.

During infiltration of ceramics by molten metals, chemical reactions, pore closure, and capillary forces due to changing wettability play important roles in controlling the flow. Wettability is defined as the ability of a liquid to spread on the solid surface [3]. Figure 2.7 shows the wettability of a liquid drop on a solid substrate. The contact angle, α, is the angle between the liquid drop and solid which is obtained from a balance of interfacial tension according to the Young-Dupre equation [75,76].

$$\gamma_{lv} \cdot \cos \alpha + \gamma_{ls} = \gamma_{sv} \qquad \textbf{2.10}$$

There are three specific energy terms: γ_{sv}, the energy of the solid/vapor interface; γ_{ls}, the energy of the liquid/solid interface; and γ_{lv}, the energy of the liquid/vapor interface.
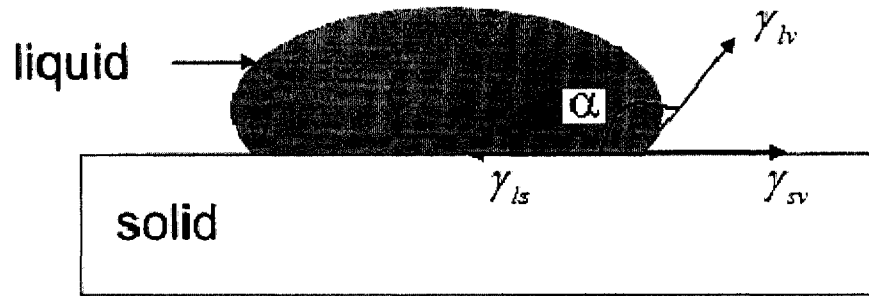
Figure 2.7: *Schematic diagram of wettability between molten metal and ceramics. I) α<90°, liquid wets solid; II) α>90°, non-wetting between solid and liquid; III) α=0 ° and α=180 ° complete wetting and non-wetting, respectively. [75,76]*

Practically, when the wettability between a molten metal and a solid ceramic is low, chemical or mechanical enhancement are recommended. Chemical enhancement can be performed either by depositing a suitable coating on the surface of the reinforcing body or by adding active alloying element(s) to the metal. The promotion agent in infiltration is essential to overcome the surface energy barrier. Kaneda and Choh [74] applied SiO_2 as the infiltration promotion agent to improve wettability between molten magnesium and SiC particles. Mechanical enhancement is achieved by applying pressure such as vacuum infiltration [70,71] and squeeze casting [19].

The penetration of a liquid (*l*) with time (*t*) through a porous material by capillary infiltration can be followed by the Washburn equation [76,22] as follows:

$$l^2 = (r\gamma_{lv} \cos\alpha / 2\eta) \times t \qquad\qquad 2.11$$

Where η is the viscosity of the liquid and r is the pore radius. A parabolic relation between time and length of infiltration has been measured in Al/TiC system at 1050 to 1200°C under flowing argon [76].

2.2.1.3 Spray Forming

Spray forming or spray deposition is a process in which the metal or alloy is melted and the liquid stream is atomized with an inert gas. Droplets of molten material are directed onto a substrate to build up bulk metallic materials [3,60]. Recently, this technique has been modified by injecting reinforcing particles in to the stream of atomized molten matrix particles (Figure 2.8). The advantageous of this method is the high rate of production. However, rapid solidification rate, which minimizes any reaction between particle and matrix, has been considered as the other advantage [3,60,78]. Some studies [78,79] on the fabrication of Mg composites using the spray forming method have been reported. Noguchi et al. [80] used the spray forming method for making Mg/SiC composites and studied the effect of SiC particle size on elastic modulus and hardness of these composites.
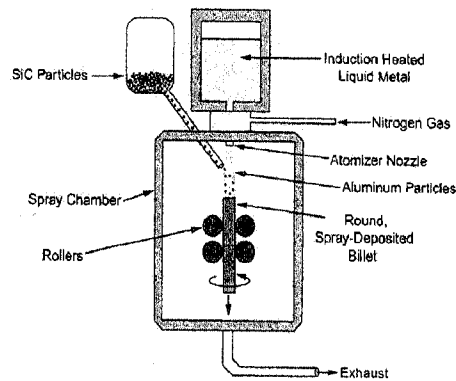
Figure 2.8: *Spray co-deposition of SiC particles and Al droplets, to form composite particles [3]*

2.2.1.4 In-situ or Reactive Process

In this technique, the reinforcing phase is formed in the matrix as a result of metallurgical reactions from the melt during its cooling and solidification. Different types of Metal

Matrix Composites have been fabricated by this method such as particle, short fiber, and long fiber reinforcing phases [81,82]. Low cost of equipment, homogeneous distribution, and good bonding between matrix and reinforcing phase are the most advantages of in-situ method. However, the reinforcing phase is limited by thermodynamic reaction [3,60]. Mg/Mg_2Si composites are probably the fist magnesium composite fabricated by this method and its analysis indicated that they have potential for elevated temperatures applications [83]. Fabrication of Mg/MgO composites has been studied for the reaction between Mg and B_2O_3 [83]. Mg/TiC composites have been formed by the reaction of Mg with Ti and C [85].

The difficulty of controlling the reinforcement to make a uniform matrix microstructure is the main disadvantage of liquid state processing. Furthermore, the reactions between matrix and reinforcement can have an adverse effect on the final properties [3]. Solid state processing is a process where the MMCs are formed by bonding of reinforcing and metal matrix phases due to mutual diffusion between them at high temperature and under pressure, in the solid state. Powder metallurgy and diffusion bonding are categorized as solid state processes [3,60]. In these techniques, the processing temperature is below (or a little above) the solidus temperature of the metallic powder. Thus, undesirable reactions on the boundary between the matrix and the reinforcing material are eliminated [3,86].

2.2.1.5 Powder Metallurgy

The metal powder and the ceramic reinforcing powder are blended, pressed, degassed, and sintered at a certain temperature and atmosphere with hot pressing or a vacuum.

Powder consolidation is one of the most popular methods to produce MMCs because of the high volume fraction of reinforcement phase (up to 70%) that can be achieved and near net shape. However, alloy powders (matrix phase) are generally more expensive than bulk material, and handling large quantities of highly reactive (potentially explosive powders) involves complicated processes. Therefore, powder metallurgy may not be a good technique for mass production of metal matrix composites [3,60,86]. AZ91/SiC, AZ91/TiO$_2$, and AZ91/ZrO$_2$ are some magnesium matrix composites fabricated by this method [87,88].

2.2.2 Processing of Aluminum Nitride Matrix Composites

Ceramic matrix composites consist of a ceramic matrix combined with a ceramic (oxides, carbides) as reinforcing phase. AlN matrix composites reinforced with other ceramics such as Al$_2$O$_3$, MgO, and Si$_3$N$_4$ have been fabricated by hot pressing, in-situ chemical reaction, reaction bonding, and DIMOX[1] techniques [23,86].

2.2.2.1 Hot Pressing

The matrix powder and fiber are mixed together and hot pressed. In this way, pore-free and fine-grained compacts will be achieved and the rate of densification will increase. The main disadvantage of this technique is non-uniformity of products due to applying unidirectional pressure. The hot isostatic pressure method at elevated temperatures has been recommended to overcome this drawback. However, it is very expensive. An example of the hot pressing technique is SiC whisker reinforced Al$_2$O$_3$, used in cutting

---

[1] Direct metal oxidation (DIMOX) as a novel technique is developed by Lanxide Corporation.

tool applications [86]. Hot pressing of mixed powders of Al-Mg and MgO to investigate the formation of $MgAl_2O_4$ phase has been reported by Kurtz et al. [57].

2.2.2.2 In-situ Chemical Reaction Techniques, Chemical Vapor Deposition (CVD) / Chemical Vapor Infiltration (CVI)

Chemical vapor deposition (CVD) is a process wherein chemical reaction or decomposition between hot substrate surfaces of the preform and a mixture of gases resulting in coating of the ceramic material on the substrate. The CVD technique has been used in some applications such as, AlN synthesis, solar cells, and refractory coating for jet engine turbine blades [24,59,86]. When the CVD technique is used for the infiltration of fiber preforms, it is termed chemical vapor infiltration (CVI) (Figure 2.9) [86]. In this method, the spaces between the fibers are filled by deposition and the matrix forms.
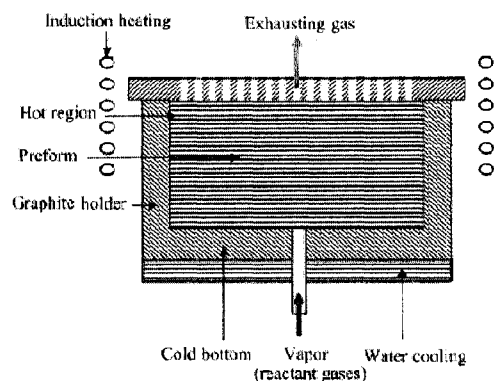
Figure 2.9: *Chemical vapor infiltration [59]*

This process has been used to fabricate near-net shape composites. Damaging the fiber reinforcement and slow process rates are the main drawbacks of the CVI technique.

Streckert et al. [89] produced SiC$_{fiber}$/SiC composites for use in fusion reactors by the CVI technique.

2.2.2.3 Reaction bonding

Reaction bonding involves reaction between a porous compact and a reactant (liquid or gas) to create a solid. In the case of gas phase reactant, the green body is made to the desired shape by compacting a mixture of the reactant (usually in the form of powders) and the reinforcing material (fibers, whiskers, or particles) [86]. The effects of processing times and temperatures on AlN/MgO, MgAl$_2$O$_4$ composite ceramic have been investigated using reactive bonding between magnesium powders and alumina preforms under nitrogen atmosphere [90]. In the case of liquid phase reactant, the reaction is between a porous solid and a liquid. For example, a porous body made by mixing SiC and C particles was infiltrated with liquid Si by Hiling et al. [91]. Aghajanian et al. [73] fabricated AlN matrix composites by infiltration of molten Al into Si$_3$N$_4$ preforms. The advantage of reaction bonding apart from near net shape fabrication is low processing temperature.

2.2.2.4 Direct melt oxidation (DIMOX)

Oxidation of a liquid metal to form a solid ceramic body using a direct growth process has been patented by Lanxide Corporation. The word DIMOX was coined by Newkirk et al. [92,93] and it stands for the DIrect Metal OXidation process. In this process, a preform of reinforcing phase (fibers, particles) is placed on the surface of the molten metal in an oxidizing atmosphere. Oxidation of liquid metal takes place in a gaseous

oxidant e.g. air. A thin layer of ceramic with some reinforcing phase will form. Capillary force acts as a driving force to infiltrate the porous ceramic layers with the melt. The melt advances and ceramic forms, this process stops when the reaction reaches the barrier as shown in Figure 2.10 [86,93,94]. Al_2O_3/SiC composites were produced by oxidation of molten Al-Mg-Si alloys into SiC powder at 1150-1350°C [94]. The DIMOX process is potentially a low-cost process with good mechanical properties. However, it is difficult to control the reaction [86]. When this process is carried out in nitrogen atmosphere with ceramic preforms such as: SiC, AlN, Al_2O_3, Si_3N_4 it is called Direct Melt Nitridation and referred to as spontaneous infiltration [72,73,95].
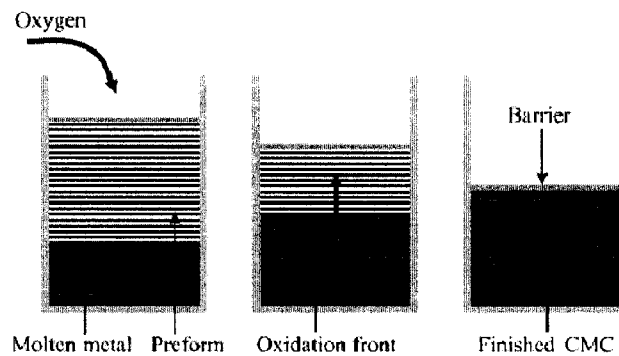
Figure 2.10: *Fabrication of CMC by DIMOX [59]*

Arroy et al. [21,22] fabricated Mg/AlN composites using sintered porous aluminum nitride ceramic particulates as preforms by infiltration of molten magnesium at 870-960°C under argon atmosphere. They studied the effects of time and temperature on the infiltration process and reported a parabolic behavior of capillary infiltration according to equation 2.11. Formation of new phases such as MgO and $MgAl_2O_4$ because of the reaction between magnesium and alumina has been detected by TEM and XRD.

Xin et al. [56] studied the effects of magnesium contents on the formation of MgO/AlN composites by spontaneous reactive infiltration of molten Al-Mg-Si alloy into preformed MgO in a pure nitrogen stream at 1200°C. They reported that Mg is vaporized and reacted with oxygen at a certain temperature, which plays a role in removing oxygen completely. On the other hand, molten aluminum infiltrated into preformed MgO and formed aluminum nitride. Spinel ($MgAl_2O_4$) phase at the interface layers has been detected by XRD and SEM.

Kevorkijan et al. [95] studied the infiltration process of molten magnesium alloy into three porous performs: quartz sand, boron carbide and silicon nitride in nitrogen atmosphere at 950°C for 4 hours by spontaneous reactive infiltration. They demonstrated that all samples have a similar spontaneous infiltration mechanism. Magnesium nitride (Mg_3N_2) formed by reaction of magnesium vapor and nitrogen atmosphere, coated the reinforcement surface and induced pressureless infiltration through greatly enhanced wetting; however magnesium nitride was not detected in final products. Formation of $MgAl_2O_4$ phase due to the reaction between SiO_2 and molten magnesium alloy at 950°C is also reported.

Hou et al. [96] reported the formation of AlN/Mg_3N_2 ceramic composites by spontaneous infiltration of aluminum into a Mg_3N_2 powder bed and found that magnesium serves as a catalyst in the nitridation process. Substitution reaction occurs between magnesium nitride and molten aluminum. Therefore, small particles of aluminum nitride were observed.

Watari et al. [90] reported a reactive infiltration of magnesium vapor into alumina powder compacts to fabricate MgO/AlN, $MgAl_2O_4$ ceramic matrix composites under

nitrogen atmosphere at 800-1000°C for 4 hours. The effects of processing time, temperature, and size of alumina particles on the densification behavior have been studied.

Kurtz et al. [57] investigated the formation of spinel ($MgAl_2O_4$) by mixing and hot-pressing of Al-Mg and MgO powders. They described the effects of heating rate, initial porosity of specimens, and MgO particle size on formation of spinel phase. They reported that Mg diffuses towards the surface of the alloy and oxidizes to form MgO which becomes available for the formation of spinel at the interface of MgO and Al-Mg.

Duncan [97] reported the formation and expansion of $MgAl_2O_4$ phase in the MgO/Al_2O_3 system through a powder metallurgy method at 1200 to 1700°C. Effects of particle size, holding time, and temperature factors on linear thermal expansion of $MgAl_2O_4$ show that an extraordinary expansion greater than the theoretical prediction, calculated from the reaction of MgO and Al_2O_3 (8.02% in volume), occurred.

Hafidi et al. [12] investigated the thermal diffusivity of various AlN-based ceramics with other sintering aids such as BeO, MgO, CaO, and Y_2O_3 using the hotpressing method. They reported that increasing oxide sintering aids, including MgO, results in lowering of the thermal diffusivity due to the formation of $MgAl_2O_4$ which acts as a thermal diffusivity barrier at grain boundaries.

Scholz et al. [98] studied Al_2O_3/Al-Mg composites at 1000°C under nitrogen atmosphere. They reported that the nitridation of pure Al in the absence of Mg was restricted to the formation of a thin protective AlN layer on Al_2O_3 which prevented further nitridation. Also, MgO and $MgAl_2O_4$ have been detected by XRD patterns.

Rao et al. [99] studied the infiltration of Al-Mg based alloy into porous alumina performs in the temperature range 800-900°C in nitrogen atmosphere. The rate of infiltration increases with reducing particle size of alumina due to increasing capillary forces. Further reduction of alumina particles to sub micron dimensions results in reducing the infiltration rate. The formation of MgO phase has been reported at 900°C.

Nagendra et al. [100] studied the mechanical properties of Al_2O_3/AlN-Al composites by pressureless infiltration of Al-Mg-Si-Fe alloys into alumina in nitrogen atmosphere. Maximum Vickers hardness of 13 GPa was achieved for samples processed in N_2-2%H_2 atmosphere at 1200°C.

In summary, the works reported on the Mg/AlN composites focused on processing of sintered AlN to produce ceramic or metal matrix composites. Nevertheless, using non-sintered AlN performs in order to approach similar density and thermal properties of sintered AlN ceramic at low temperature could not be found in the literature.

2.3 Objectives of the Present Work

Nowadays, the demand for high thermal conductivity aluminum nitride is high and many studies focus on increasing its thermal conductivity with low cost techniques. In fact, all known techniques for sintering aluminum nitride are expensive due to high temperatures (> 1700 °C) and long processing times.

To date, no effort has been made to study spontaneous infiltration of molten magnesium alloys into non-sintered aluminum nitride at low temperature (<1000°C) to

achieve a thermal conductivity similar to sintered AlN ceramic. The main objectives of this work are to:

- Establish a method for pressureless infiltration of magnesium into non-sintered aluminum nitride at low temperatures, making a dense composite.

- Assess the phase development and stability in the AlN/Mg system at various temperatures in the range 650 to 950°C under nitrogen atmosphere using room temperature X-ray diffraction.

- Characterize the microstructure of products in terms of porosity and formation of new phases due to in-situ reaction.

- Calculate thermal conductivity based on thermal diffusivity, density, and heat capacity measurements by laser flash, Archimedes law, and differential scanning calorimetry, respectively.

CHAPTER 3: EXPERIMENTAL PROCEDURE

The present work involves the pressureless infiltration of molten AZ91E magnesium alloy into non-sintered aluminum nitride porous preform. The experimental work consists of:

1- Set-up experimental facilities such as: die and punch to make compact preform, cylindrical chamber, inlet, and outlet pipes to apply nitrogen gas.

2- Fabricate aluminum nitride composite by infiltration of molten magnesium alloy (AZ91E) into AlN preforms.

3- Carry out the microstructural, physical, and thermal characterization of the products.

Figure 3.1 shows the experimental procedure with all the steps that will be discussed in the following sections.
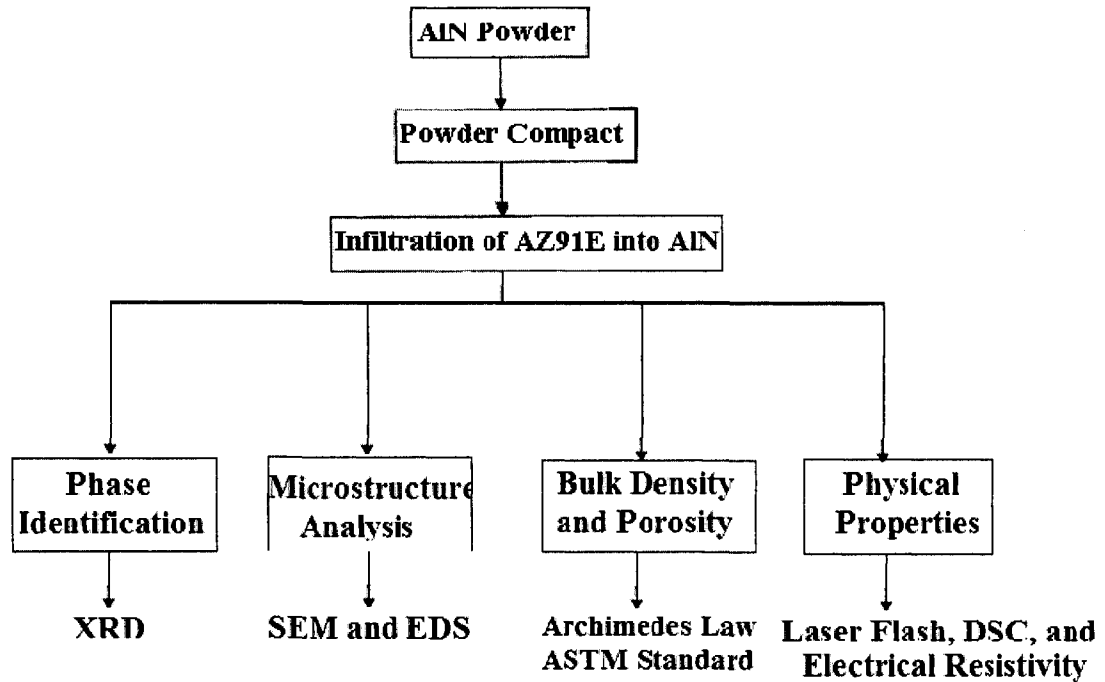
Figure 3.1: *Experimental procedure flow chart*

3.1 Raw Materials

3.1.1 Aluminum Nitride

All experiments were employed using AlN powder, dry-pressable grade, supplied by Accumet Materials Co., USA, containing 5 wt.% Yttria, 1 wt.% Oxygen, 0.08 wt.% Carbon, 50 ppm Iron, 40 ppm Silicon and 80 ppm other impurities. The average particle size of the powder is 4-5 microns.

3.1.2 Magnesium Alloy, AZ91E

The AZ91E alloy with 648±3 °C melting point was used in the present work provided by MEL (Magnesium Elektron, Manchester, UK) and its chemical composition is given in Table 3.1.

Al	Mn	Zn	Mg
8.1~9.3	0.17~0.35	0.4~1.0	balance

3.2 Composite Fabrication

3.2.1 Preform Preparation

The particles were poured into a 25 mm diameter die and uniaxially pressed by hydraulic force at a pressure 50-70 kPa in order to make a compact powder disc. Preform dimensions were maintained at 25mm diameter and between 6~10 mm heights. Figure 3.2 shows the drawing of die and punch used to make the preform.
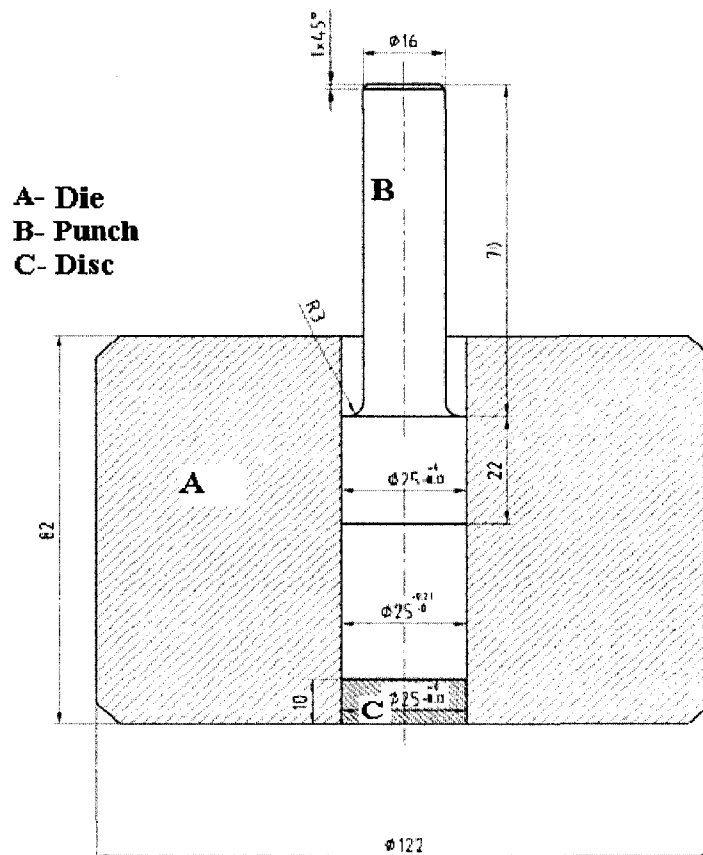
Figure 3.2: *Drawing of the die and punch used to make AlN Preform. All dimensions are in mm; A- Die, B- Punch, C- Disc*

3.2.2 Alloy Preparation

Magnesium alloy ingot was cut into round shapes by saw in order to cover the preform disc. All sides were polished with 120 and 240 grit SiC papers to remove oxygen layers. Samples were immersed in hydrofluoric (HF) acid and cleaned in acetone right before the infiltration experiment in order to minimize oxidation.

3.2.3 Infiltration Equipment

The equipment for the infiltration process to fabricate AlN composites consists of:

1. LINDBERG/BLUM 1100°C box furnace (model: BF5-1800) equipped with 16 segment programmable controller and K-type thermocouple to control temperature inside the furnace.

2. Magnesium alloys and AlN preforms were placed in a boron nitride crucible and surrounded by a powder bed of AlN in order to facilitate removal of the composite and residual metal after the experiment.

3. A cylindrical iron chamber and relevant pipes to introduce nitrogen gas (about 1 cm³/min.) into the chamber during heating up surrounded the BN crucible.

3.2.4 Infiltration Processing

In order to achieve full infiltration, simultaneous downward and upward infiltrations have been employed. The boron nitride crucible containing the aluminum nitride preform and two pieces of magnesium alloy (AZ91E), on the top and bottom of the preform, were carefully placed in the furnace (Figure 3.3). The mass fraction of AlN to Mg was kept constant at 5/3 (Table 3.2). Experiments were performed at three temperatures (650°C,

800°C, and 950°C) for different times (25, 60, 90, and 135 min.). Afterwards, the furnace cooled down to room temperature. Figure 3.4 shows the temperature profile applied in these experiments.

Table 3.2: *All samples and relevant mass fractions*

Samples Processed at		AlN/Mg mass fraction ($\approx$5/3)
Temp. (°C)	Time (min)	
650	25	6.15/3.8
650	60	5.16/3.11
650	90	3.98/2.40
650	135	11.224/7.01
800	25	5.46/3.36
800	60	3.46/2.1
800	90	4.87/2.89
800	135	4.61/2.89
950	25	4.98/2.89
950	60	5.23/3.3
950	90	4.36/2.7
950	135	15.46/9.56
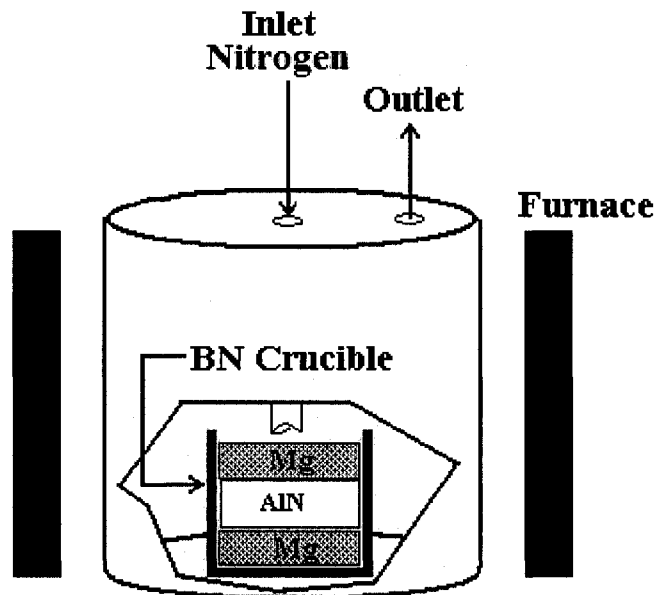
Figure 3.3: *Schematic set up for upward and downward infiltration of two pieces Mg alloys into AlN preform inside BN crucible*
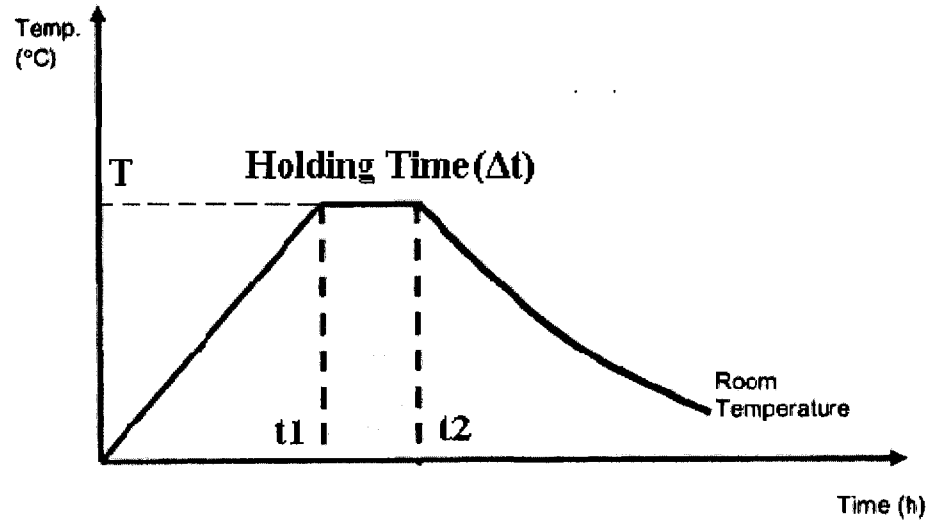
Figure 3.4: *Experimental temperature profile with 4 °C/min. heating rate: $\Delta t = t_2 - t_1$ (25,60,90, and 135 min), $T = 650$, 800, and 950 °C*

3.3 Composite Characterization

3.3.1 Density and Porosity Measurements

The bulk density of the infiltrated composites was measured by Archimedes method, as stated in ASTM standard C20-97 [102]. The dry weight (D) was measured, and then the sample was placed in boiling water for 2 hours. After boiling, the specimens were cooled to room temperature while still entirely immersed in water for 12 hours. Each specimen was weighed while being suspended in water (S). Then, the weight of wet samples was measured in air (W). The following equations were used to calculate the apparent porosity (P) and bulk density (ρ_B):

$$P(\%) = \frac{W-D}{W-S} = \frac{W-D}{V} \times 100 \qquad \text{3-1}$$

$$\rho_B = \frac{D}{W-S} = \frac{D}{V} \qquad \text{3-2}$$

V is called the exterior volume in cubic centimeters knowing that 1 cm³ of water weights 1 g.

3.3.2 Bulk Electrical Resistivity Measurements

The Agilent 4339B high-resistance meter for making precision high-resistance measurements was used, at room temperature. Electrical contacts were made with thin layer of highly conducting silver adhesive on the top and bottom of each sample (Figure 3.5).

Silver Adhesive Both Sides
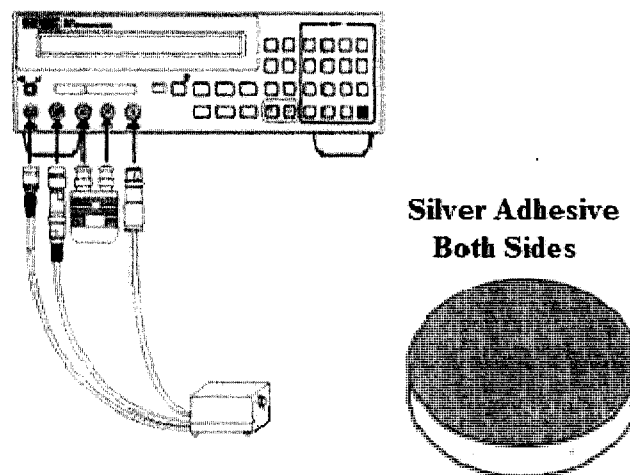
Figure 3.5: *Experimental setting for electrical resistivity measurement*

3.3.3 Sample Preparation

The samples were sectioned into several portions as shown in Figure 3.6. All pieces were cut by a BUEHLER ISOMET low speed saw machine. Section "B" was cut into more pieces used for scanning electron microscopy, X- ray diffraction, and differential scanning calorimetery. Section "A" was cut into a square shape (12.5mm×12.5mm and 2-

3 mm thickness) to measure thermal diffusivity. Section "C" and "D" were used for density and porosity measurements.
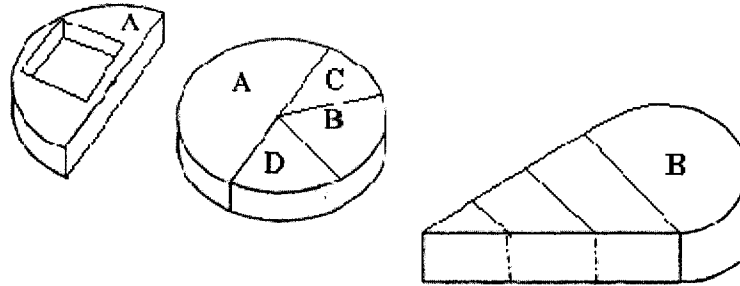
Figure 3.6: *Schematic sample preparation process*

3.3.4 Sample Preparation for Microanalysis

Samples were ground with 120, 240, 400, 600, 800, and 1200 grit SiC papers, and polished following this process; samples were polished by soft synthetic short-napped fiber cloth using 9 and 1 micron diamond pastes with water as lubricant and coolant [103]. The polishing was finished with 0.05 micron colloidal silica.

3.3.5 Scanning Electron Microscopy

The microstructure of the composites was examined by JEOL JSM-840A scanning electron microscope (SEM) equipped with Energy Dispersive X-ray Spectroscopy (EDS) in the Mining and Material Engineering Department of McGill University. The SEM was used either in the secondary electron (SEI) or backscatter electron (BSE) modes at 15 KeV. A thin layer of gold-palladium coating to enhance conductivity of the samples for imaging purposes in case of surface charging was used.

3.3.6 X-Ray Diffraction (XRD)

In order to determine the crystalline phases in the composites, a CuK_α X-ray diffractometer (APD 1700, Philips) in the Mining and Material Engineering Department of McGill University, was used. The analysis was performed at an accelerating voltage of 40 KV (±0.1%) and a beam current of 20 mA (±0.1%) for 2θ angles of 5 to 85°.

3.3.7 Thermal Conductivity

Once thermal diffusivity and heat capacity (C_p) are obtained, the thermal conductivity can be calculated according to:

$$K = C_p \times \rho \times D \qquad\qquad \text{3-3}$$

Where;

  K = Thermal conductivity (W/mK)

  C_p = Specific heat capacity (J/gK)

  ρ = Density of samples (kg/m³)

  D = Thermal diffusivity (m²/s)

Therefore, to calculate the thermal conductivity of samples, measurement of thermal diffusivity and heat capacity as well as density is required.

I) Thermal Diffusivity Measurements

Thermal diffusivity of samples was determined by means of a laser nano-flash apparatus (NETZSCH, LFA 447) using a Xenon flash lamp operating at 400 ms and liquid nitrogen as coolant. To analyze thermal diffusivity, the composite samples were cut in the form of 12.5mm square slabs with approximately 2-3mm thickness. Both faces of each sample

were coated by a thin layer of graphite to ensure uniform absorption of laser beam. The finite pulse correction of Cowan (see appendix A) was applied to the measurements.

II) Heat Capacity Measurement

Heat flux Differential Scanning Calorimetry (DSC) (TAinstruments-Q10) was used to measure heat flow vs. temperature between 25 to 300°C with 0.34°C/Sec heating rate. Before acquiring the measurement of heat flow, each sample was heated twice up to 350°C and then cooled to make sure samples had no moisture. Based on the following relation between heat capacity (C_p) and heat flow (dH/dt), the C_p can be calculated:

$$\frac{dH}{dt} = C_p \frac{dT}{dt} + f(T,t) \qquad\qquad \textbf{3-4}$$

Where;

dH/dt = Heat Flow (W/g)

Cp = Heat capacity (J/ ° C)

dT/dt = Heating rate (° C/Sec)

f(T,t)= Heat flow as function of time and temperature
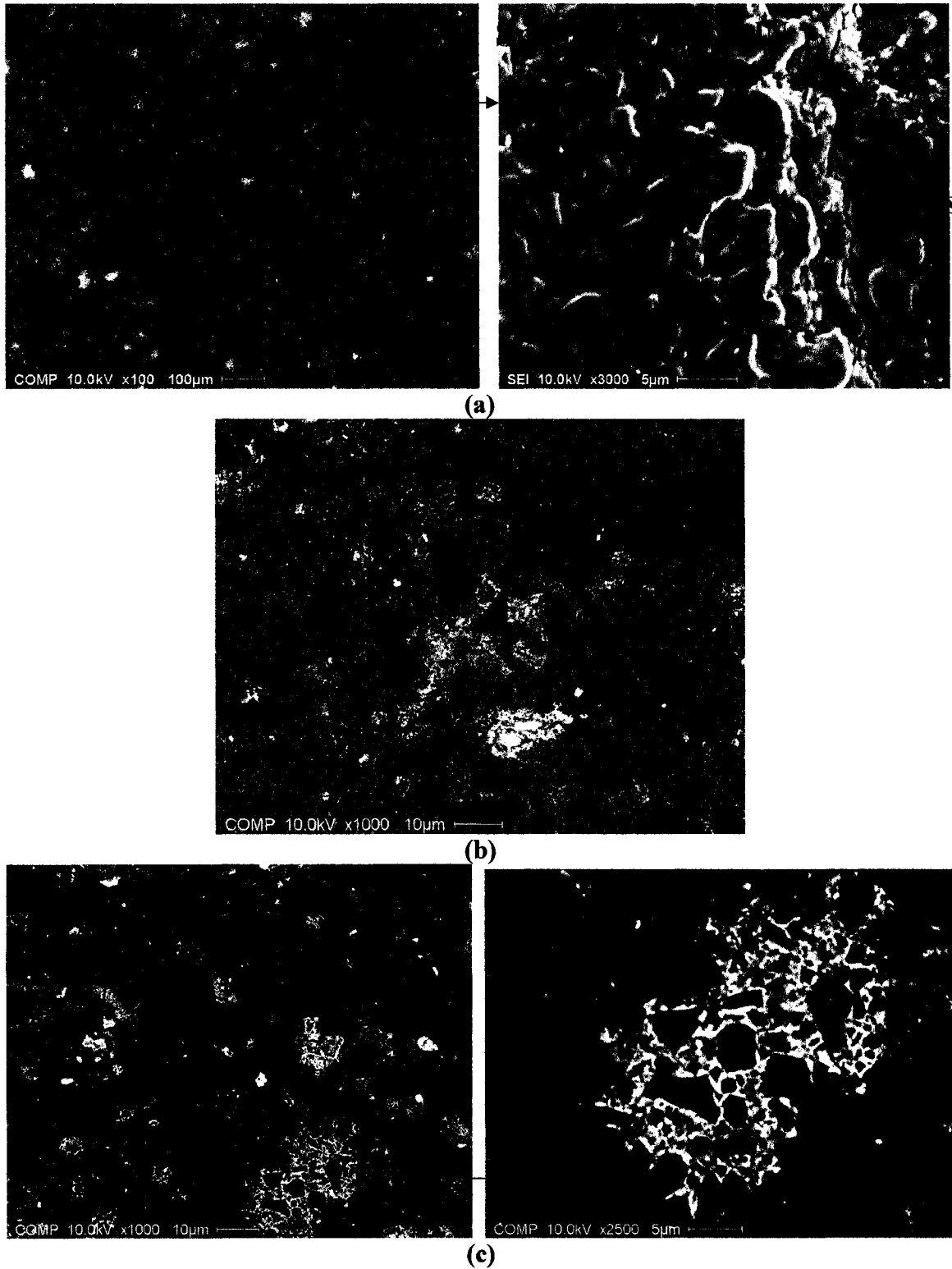
Figure 4-1: *SEM micrographs of samples infiltrated at 650 ℃; a) 25 min., b) 90 min.*
c) 135 min. Region "A" AlN, Bright spots "B" metallic phase

magnesium are detected at all holding times. Gamma phase ($Mg_{17}Al_{12}$) peaks have been observed only in samples with holding times 90, and 135 min. However, the gamma phase peaks are not as strong as that of aluminum and magnesium.

The resulting composite at this temperature contained metallic phases as can be seen in Figure 4.3. The existence of metals in the final composite indicates incomplete oxidation and nitridation, thus the ceramic matrix composite formed is unsuitable for electronic applications.
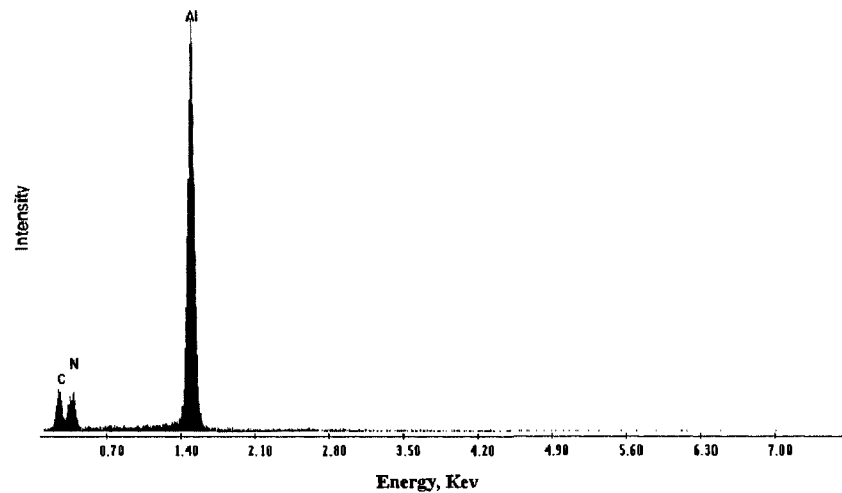
(a) Regions "A"
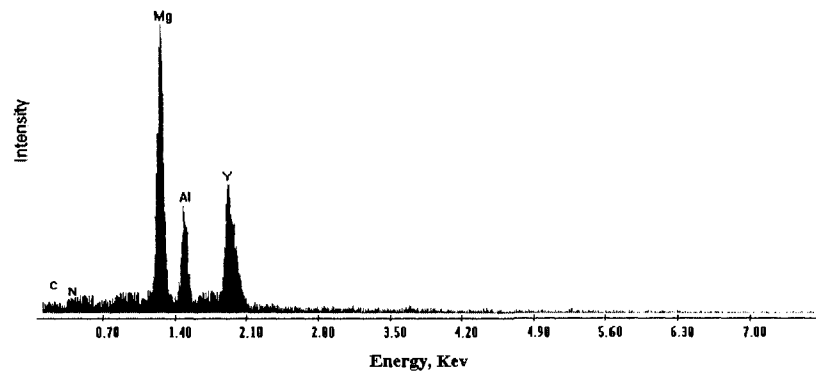
(b) Bright Spots "B"

Figure 4-2: *EDS patterns corresponding to the regions with different color and morphology in Figure 4.1; a) dark region, b) bright spots*
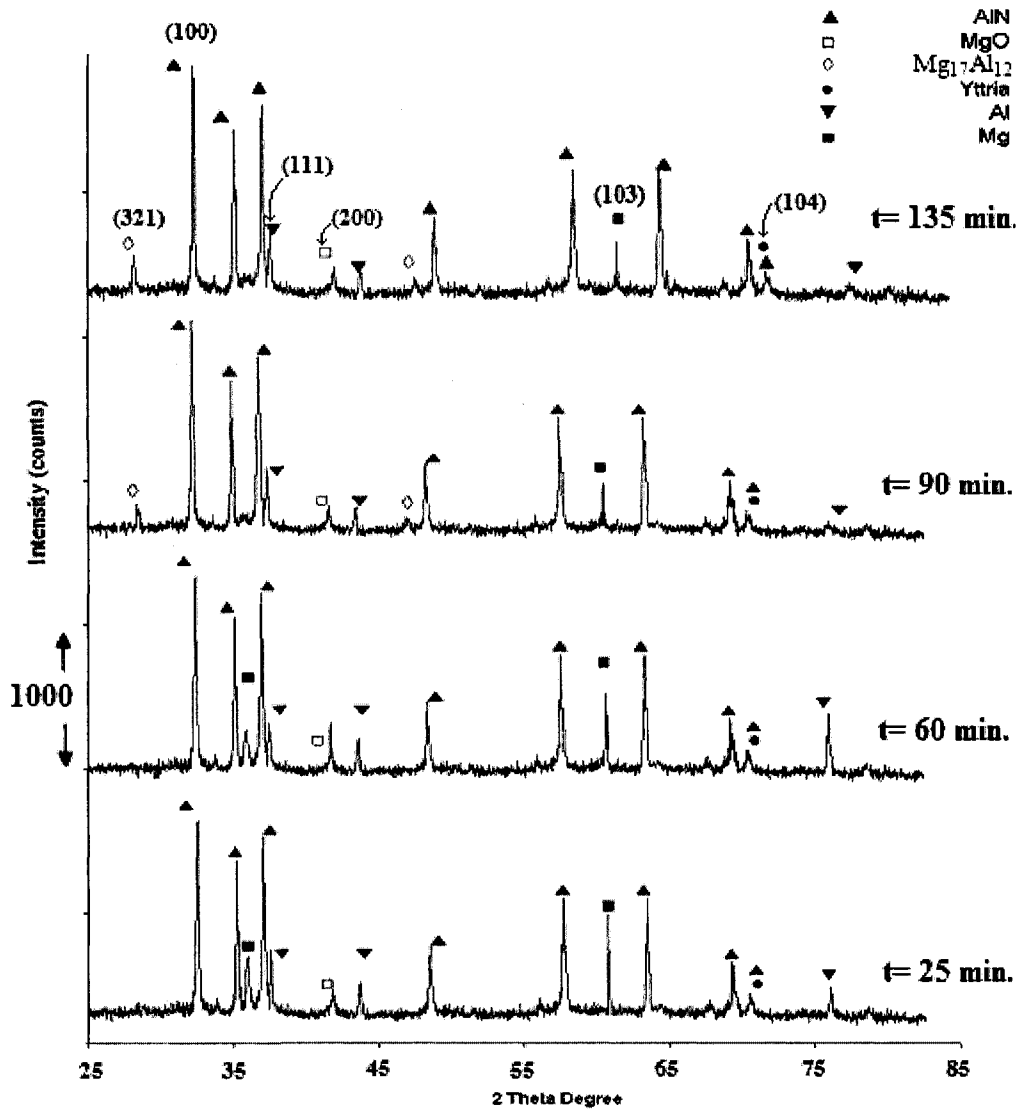
Figure 4-3: *XRD patterns for infiltration at 650°C with different holding times*

Formation of $Mg_{17}Al_{12}$ takes place during solidification at 458°C (731K) based on the Al-Mg phase diagram shown in Figure 4.4. EDS results in most regions of the AlN show that a thin layer of metal covered the edges of the aluminum nitride regions. Figure 4.5 shows a representative interfacial region.
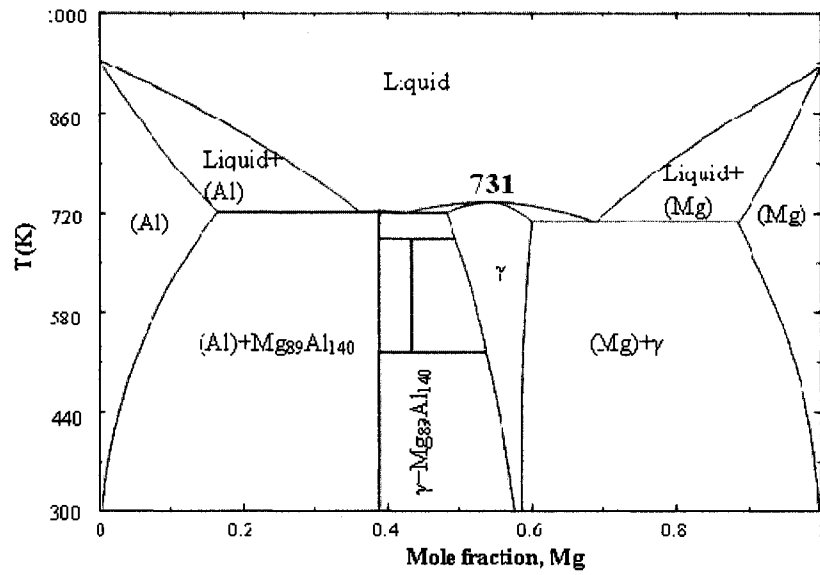
Figure 4-4: *Al-Mg Phase Diagram [101]*
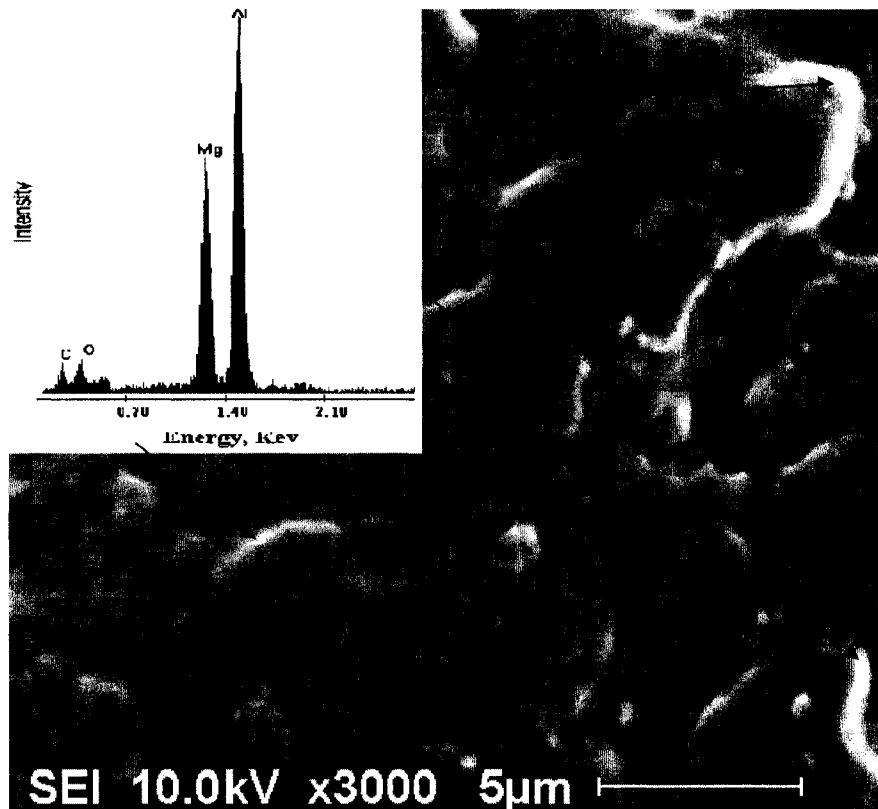
Figure 4-5: *Typical interfacial region of composite and EDS result for samples infiltrated at 650°C*

The effects of holding time on the phase contents were investigated by the peak ratio technique. The results are shown in Figure 4.5. The peak ratio is defined as:

$$(l_{hkl} / l_t) \times 100 \qquad\qquad \textbf{4-1}$$

Where l is XRD intensity and l_t is:

$$l_t = l_{100(AlN)} + l_{200(MgO)} + l_{321(Mg_{17}Al_{12})} + l_{104(Y_2O_3)} + l_{111(Al)} + l_{103(Mg)} \qquad \textbf{4-2}$$

l_{hkl} is the highest peak for each phase in a given XRD pattern. For instance, crystallographic data [104] for the current experimental XRD pattern show that the highest peak for AlN occurs for the (111) plane. Figure 4.6 revealed that as holding time increases, the quantity of MgO slightly increases and the amount of gamma phase increases as well. However, the quantity of aluminum nitride and aluminum phases is almost constant. Magnesium reduces due to evaporation and oxidation.
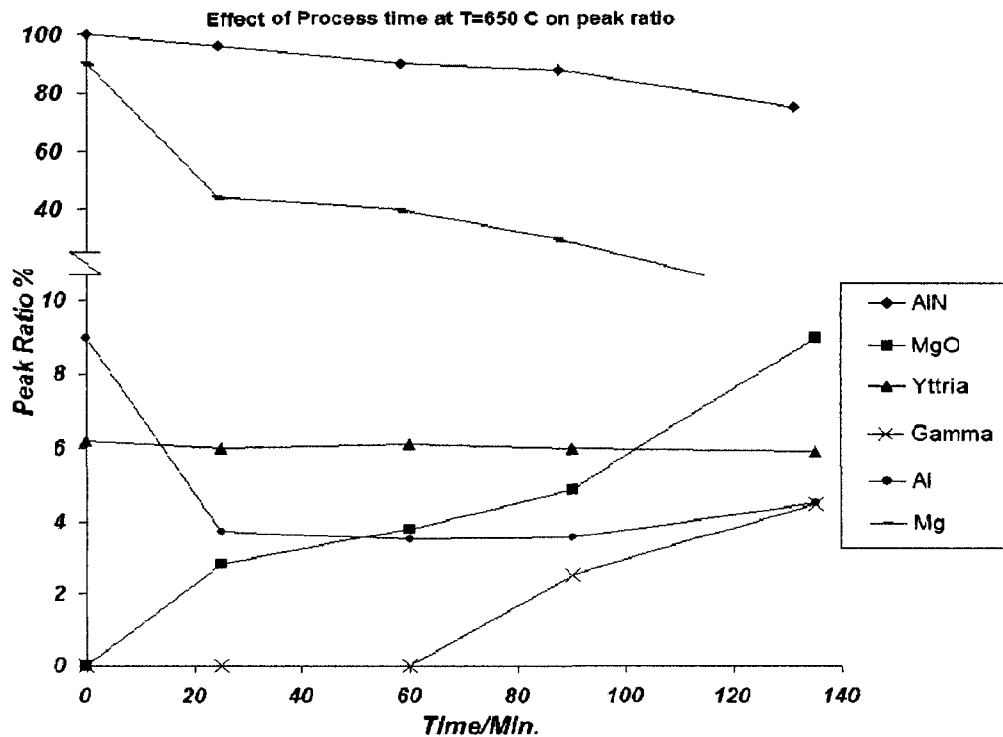
Figure 4.6: *Effect of holding time on the phase contents of samples processed at 650°C*

According to these results, it is suggested that in the initial stages, some amount of magnesium volatizes at 650°C and reacts with nitrogen and both gaseous magnesium nitride and magnesium vapor forms. Magnesium vapor pressure (2.9 KPa at 650°C) is relatively higher than that of magnesium nitride (3.9×10⁻³ Pa at 650°C). Furthermore, the Gibbs free energy of MgN formation is positive:

$$Mg + \frac{1}{2}N_2 \rightarrow MgN \qquad \Delta G>0 \qquad \textbf{4-3}$$
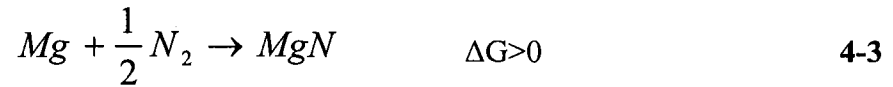
Therefore, only magnesium could be considered as an active vapor phase in this process and it reacts with oxygen:

$$Mg + \frac{1}{2}O_2 \rightarrow MgO \qquad \Delta G= -96.8 \text{ KJ} \qquad \textbf{4-4}$$
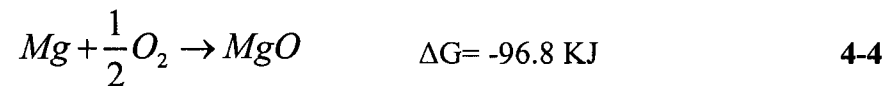
The remaining part of the magnesium alloy infiltrated into the AlN preform. The quantity of AlN almost remains constant because the temperature is still lower than the oxidation of the AlN which is more than 700°C [46]. On the other hand, XRD patterns of AlN powder after several refinements show that only 1.04 wt % alumina exists in AlN powder (Figure 4-7). Thus, MgO forms mainly through the oxidation of magnesium (Equation 4-4) and it grows slightly with increasing holding time.
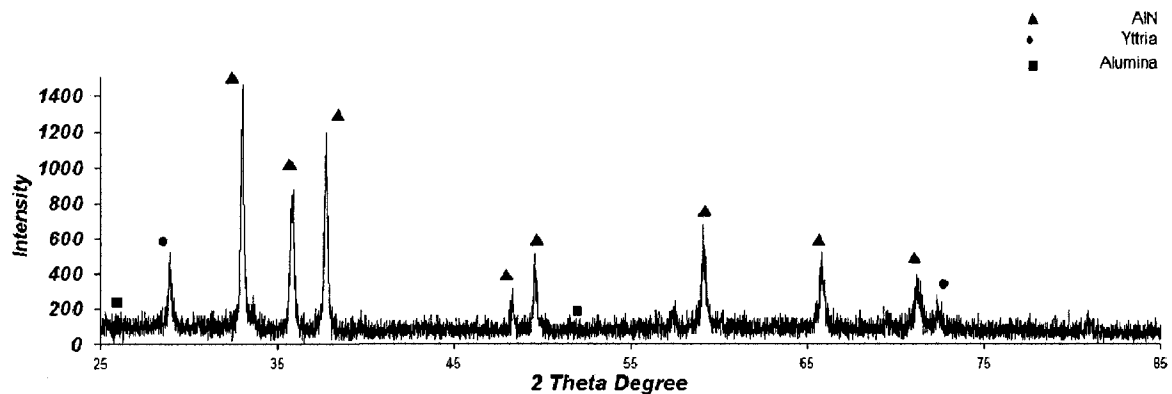
Figure 4-7: *XRD pattern of raw AlN powder*

II) Composites Fabricated at T= 800 °C

The infiltration experiments were successfully carried out at 800°C and four holding times (25, 60, 90, and 135 min). Except for the sample with a holding time of 25 min, which was fragile and porous, the other samples were relatively strong and dense. Figure 4-8 shows SEM images of samples processed at different holding times. Pores and microcracks are indicated on the images. EDS patterns in Figures 4-9 show that regions "**A**" consist of aluminum, nitrogen, and some amount of yttrium while particles "**B**" are composed of magnesium and oxygen. XRD patterns in Figure 4-10 support the EDS results and revealed that samples with 25 min, 60 min, and 90 min holding times are composed of two distinct phases, aluminum nitride and magnesium oxide. In addition to the presence of AlN in regions "**A**", small AlN particles have also been observed through the SEM images (Figure 4-8a,b). The sample that was kept at 800°C for 135 min. holding time consists of spinel phases ($MgAl_2O_4$) in addition to aluminum nitride and magnesium oxide. However, the XRD peaks of spinel are weak compared to other peaks and due to relatively small amount, it could not be observed in the SEM images. The phase diagram of alumina and magnesia (Figure 4-10) shows that formation of spinel occurs at a higher temperature than 792 °C.
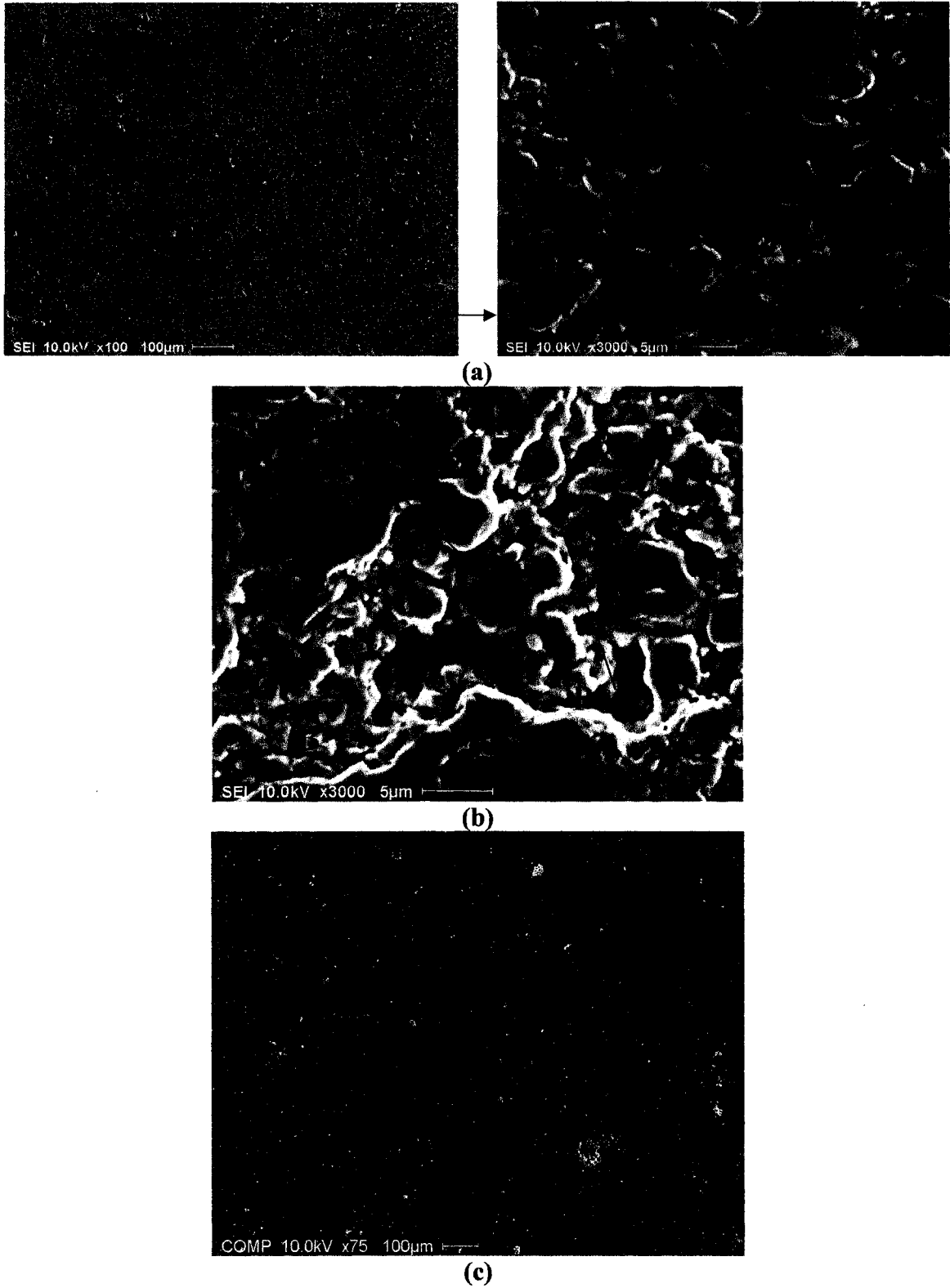
Figure 4-8: *SEM micrographs of samples infiltrated at 800°C for: a) 25min , b) 90 min c) 135 min*
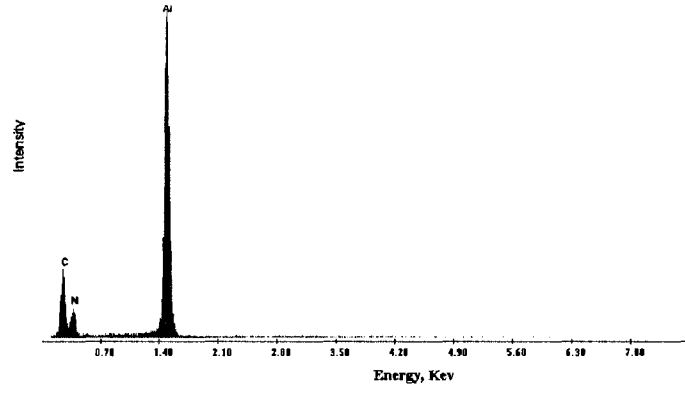
(a)
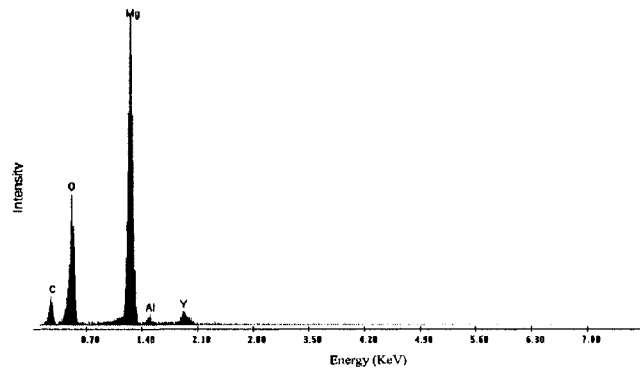
(b)

Figure 4-9: *EDS pattern corresponding to: a) Regions "A", b) Regions "B" in Figure 4-7*
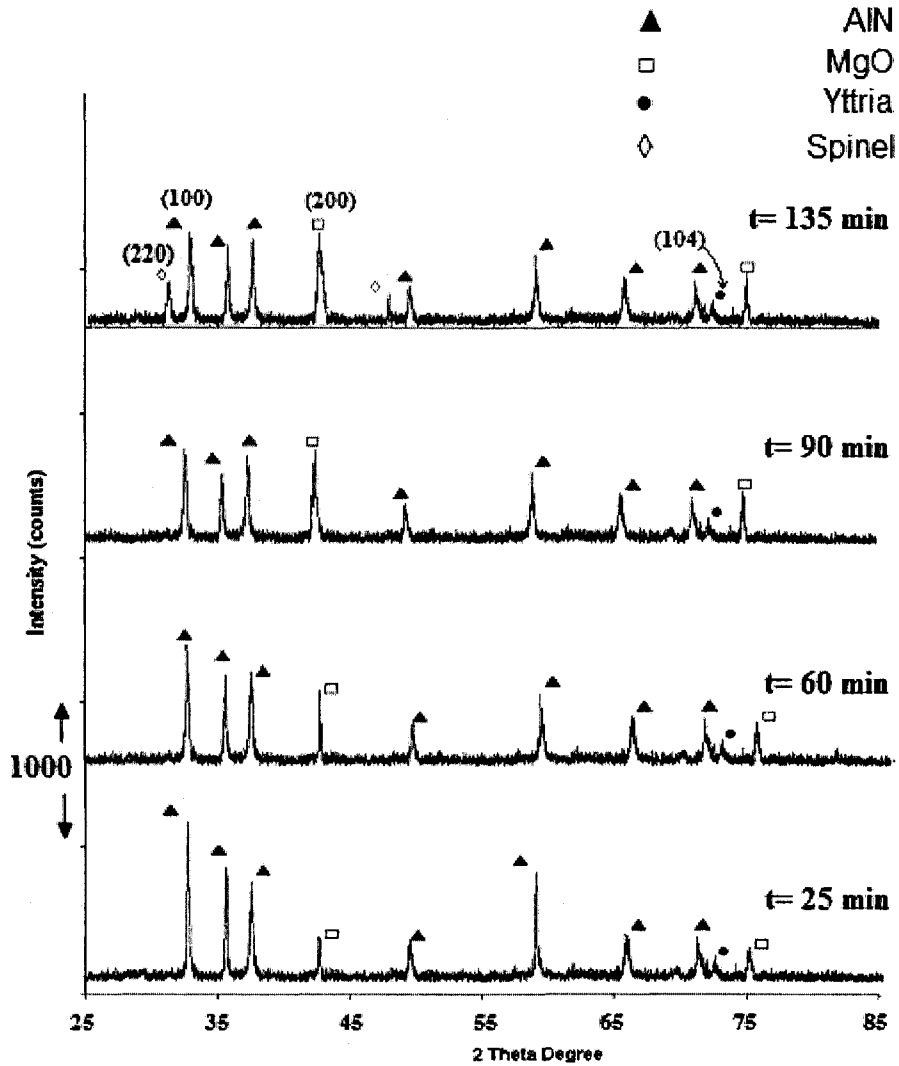
Figure 4-10: *XRD patterns for infiltration at 800°C and different times*

The effects of process time on the phase contents indicate that as holding time increases, the amount of AlN is reduced and the magnesium oxide content increases (Figure 4-11). The peak ratio has been calculated using:

$$It = I_{100(AlN)} + I_{200(MgO)} + I_{104(Y_2O_3)} + I_{220(MgAl_2O_4)}$$

4-5
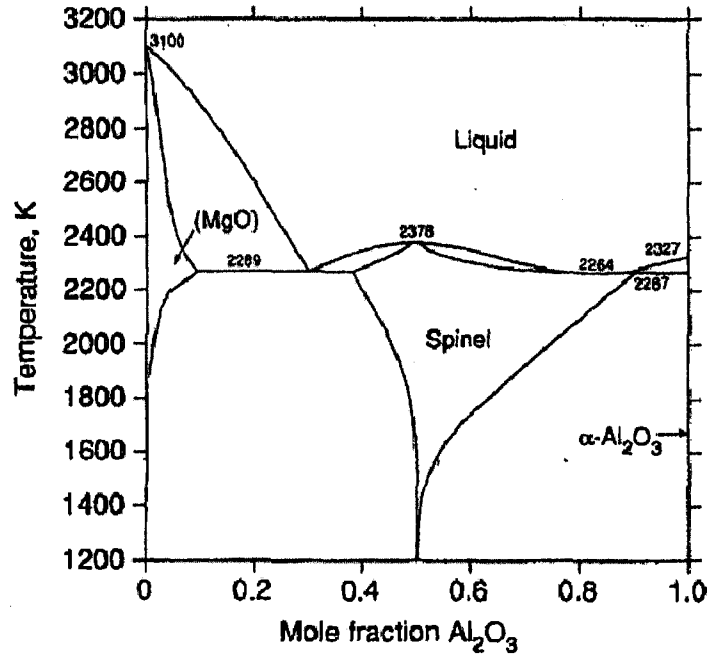
Figure 4-11: Al_2O_3-MgO Phase Diagram [110]

Based on all results, it is suggested that, similar to the composite samples at 650°C, magnesium reacts with oxygen and forms magnesium oxide. Furthermore, aluminum nitride starts to oxidize beyond 750°C [87,89] and alumina forms according to the following reaction:

$$4AlN(s) + 3O_2 \rightarrow 2Al_2O_3 + 2N_2 \qquad \textbf{4-6}$$
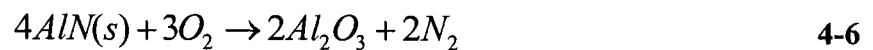
Formation of more magnesium oxide is attributed to the reaction of the alumina film with magnesium according to Equation 4-7. Therefore, the rate of MgO formation is higher than observed for the samples processed at 650°C.

$$Al_2O_3(s) + 3Mg(g) \rightarrow 2Al(l) + 3MgO(s) \qquad \textbf{4-7}$$
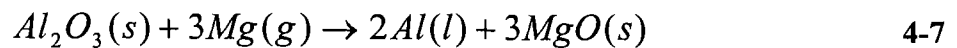
No metals were observed in the samples processed at 800°C with 25, 60, 90, and 135 min holding times. Some of the liquid aluminum formed according to Equation 4-7, reacts with nitrogen to form aluminum nitride according to:
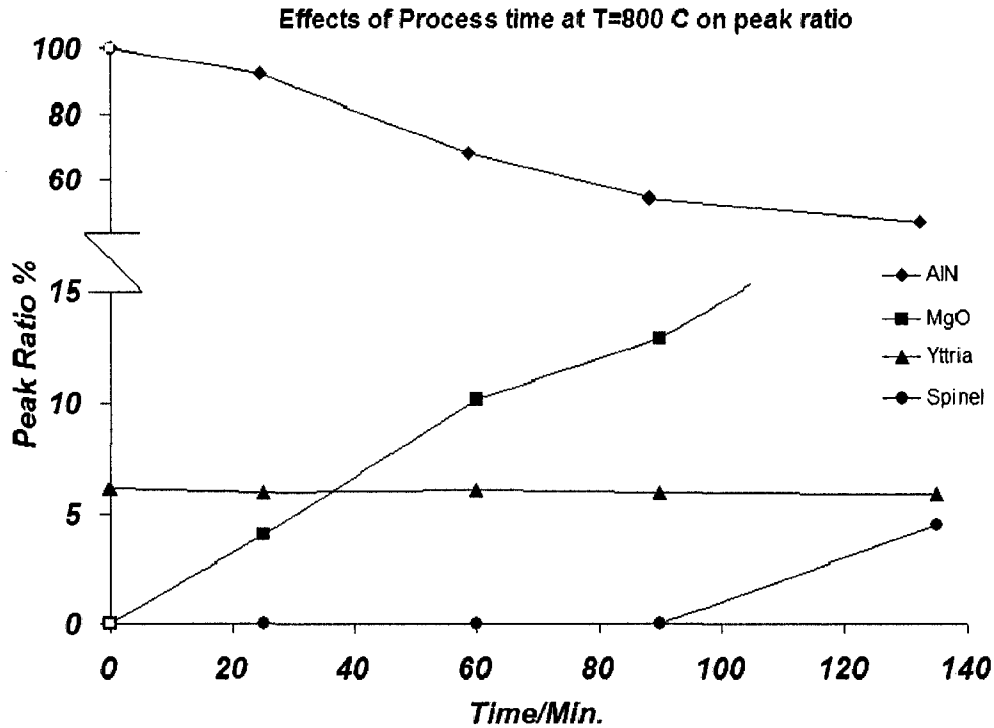
Figure 4-12: *Effect of holding time on the phase contents of samples processed at 800°C*

$$2Al(l) + N_2(g) \rightarrow 2AlN(s) \qquad\qquad \textbf{4-8}$$
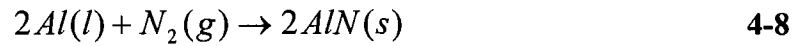
Formation of spinel ($MgAl_2O_4$) occurs only in the sample with 135 min holding time because of the reaction of alumina with magnesium oxide as:

$$MgO(s) + Al_2O_3(s) \rightarrow MgAl_2O_4 \qquad\qquad \textbf{4-9}$$

III) Composites Fabricated at T= 950 °C

SEM images of samples at four different holding times are shown in Figure 4-13. The infiltration experiments were successfully carried out at 950°C with four holding times (25, 60, 90, and 135 min).
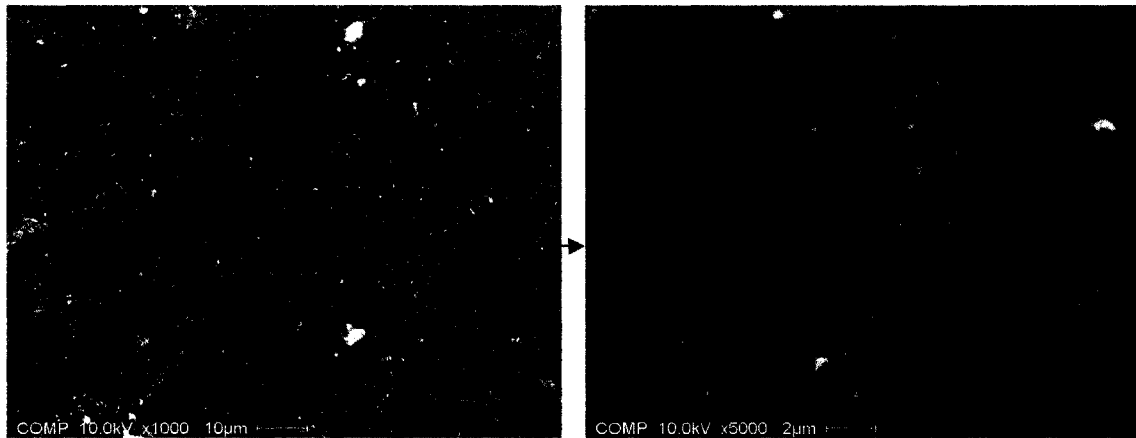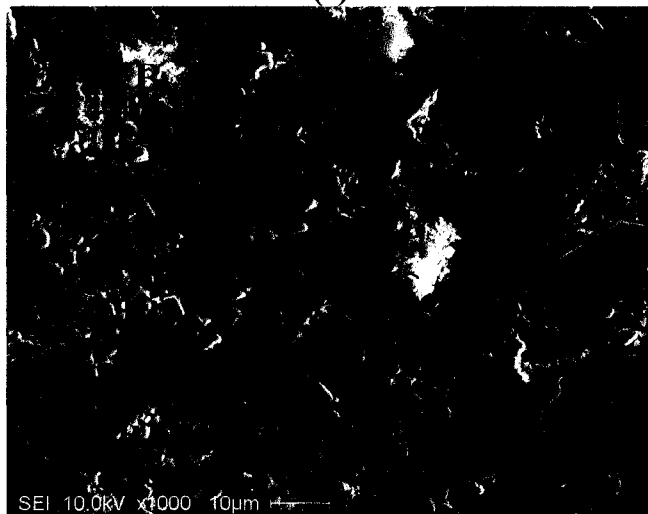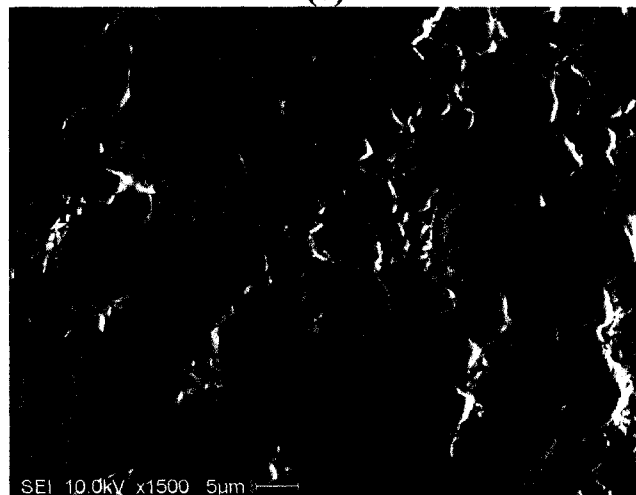
Figure 4.13: *SEM micrographs of samples infiltrated at 950 °C; a) 25 min, b) 90 min c) 135 min*

All samples were relatively denser than the ones processed at lower temperatures. Pores and microcracks are pointed out on the SEM images and relatively more uniform distribution of aluminum nitride is observed compared to other samples. EDS and XRD patterns are shown in Figure 4-13 and 4-14, respectively.

(a)

(b)

(c)
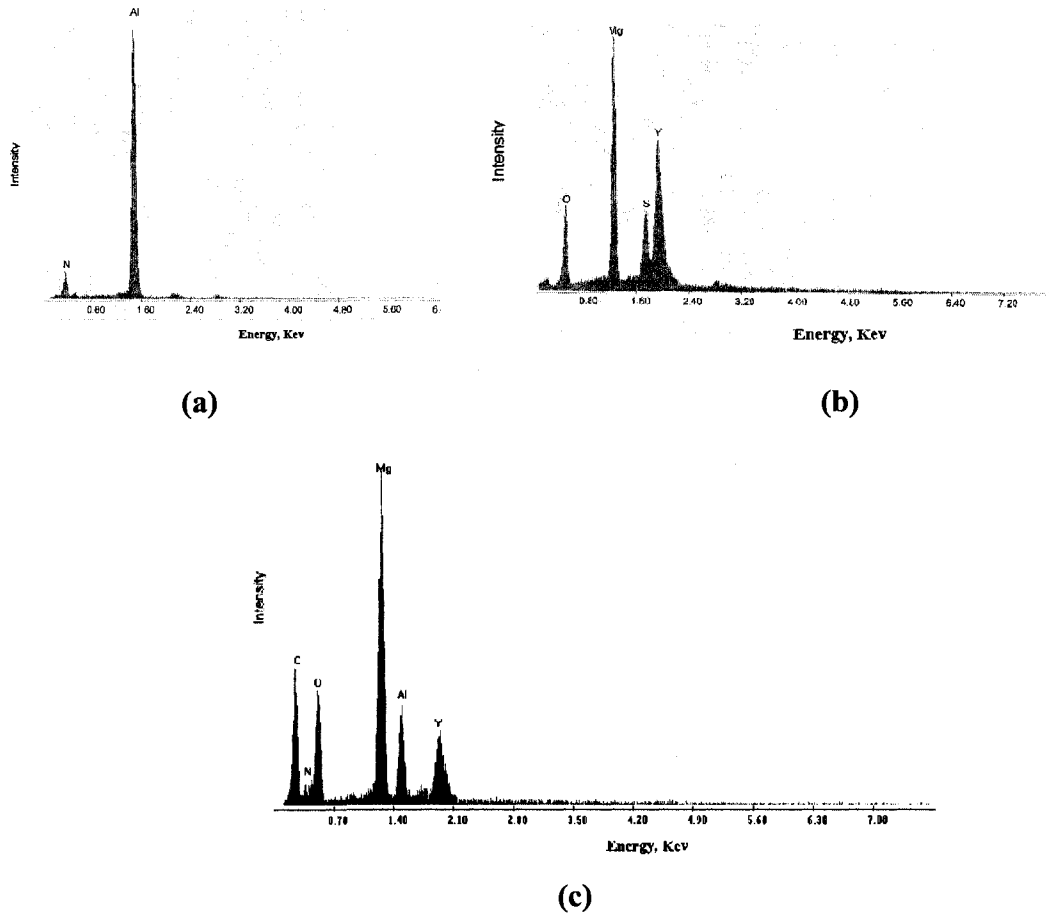
Figure 4-14: *EDS pattern corresponding to: a) Regions "A", b) Regions "B", c) particle "C" in Figure 4-12*

Samples with 25 min and 60 min holding times have two phases, aluminum nitride (region "A") and magnesia (particles "B"). However, some tiny AlN particles have been detected through SEM (Figure 4-13b,c).
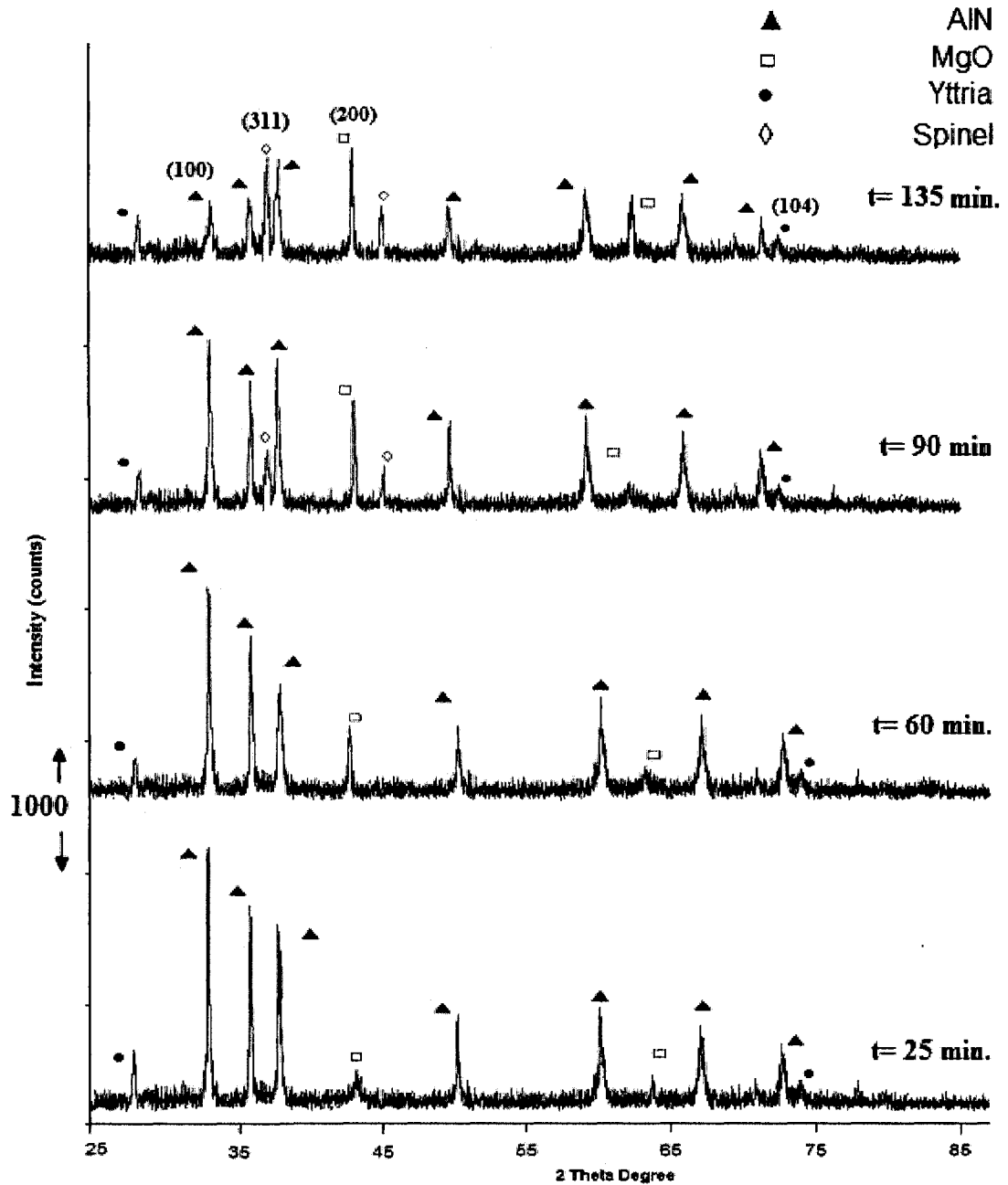
Figure 4.15: *XRD patterns at 950 °C and different holding times*

Samples with 90 min and 135 min process time consist of three distinct phases; aluminum nitride, magnesia, and spinel ($MgAl_2O_4$) in region "C". This is supported by the XRD patterns in Figure 4.15 which shows relatively strong spinel peaks in samples processed at 135 min.

Effect of processing time is presented in Figure 4.16. Peak ratio has been calculated by:

$$It = I_{100(AlN)} + I_{200(MgO)} + I_{104(Y_2O_3)} + I_{311(MgAl_2O_4)} \qquad \textbf{4-10}$$

As time increases, the quantity of aluminum nitride decreases due to its oxidation. On the other hand, formation of magnesia and spinel increase according to equations 4-7 and 4-9. In the samples processed at 950 °C, formation of spinel occurs at lower holding times (90 min) compared to 135 min for the case of 800°C. The rate of magnesia formation and aluminum nitride consumption are higher than at 800 °C.
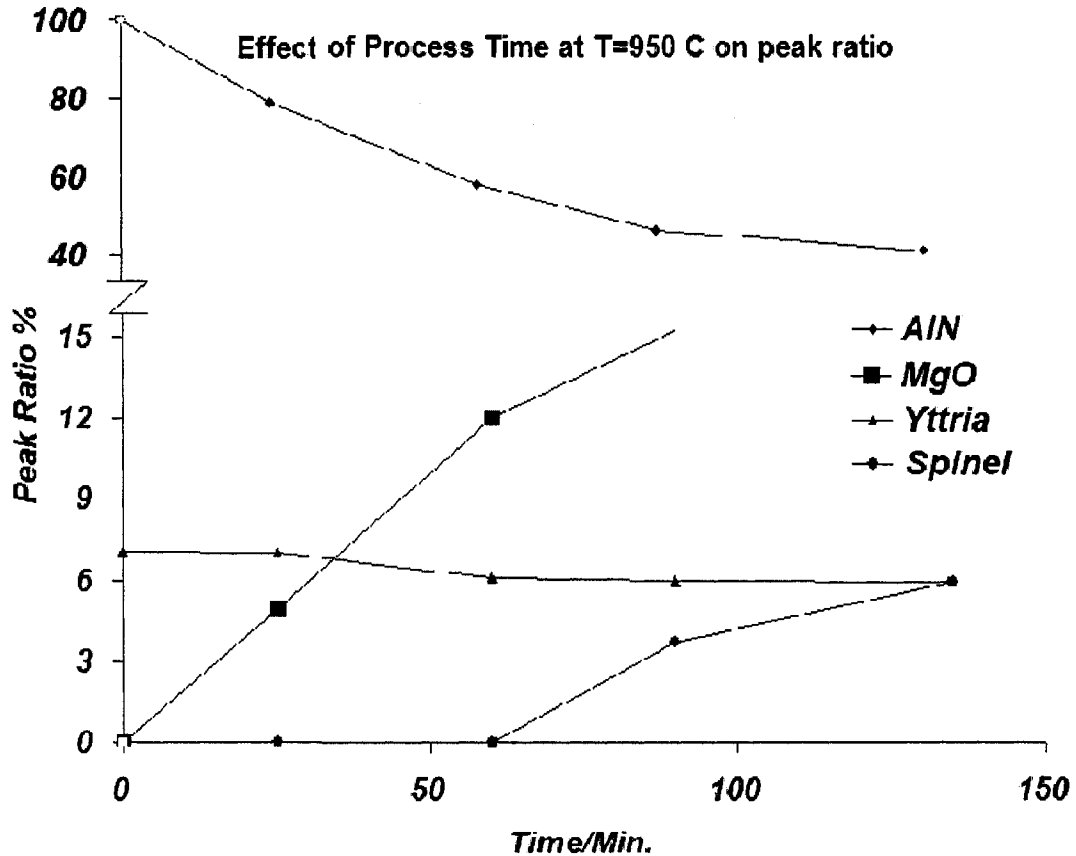
Figure 4.16: *Effect of holding time on the phase contents of samples processed at 950 °C*

58

4.2 In situ Infiltration Mechanisms

The kinetics of the spinel formation reaction was first quantitatively described by Wagner [105] and Carter [106]. They reported that in the MgO/Al_2O_3 system, one quarter of $MgAl_2O_4$ spinel forms at the $MgO/MgAl_2O_4$ interface, while three quarter forms at the $MgAl_2O_4/Al_2O_3$ phase boundary (Figure 4-17).
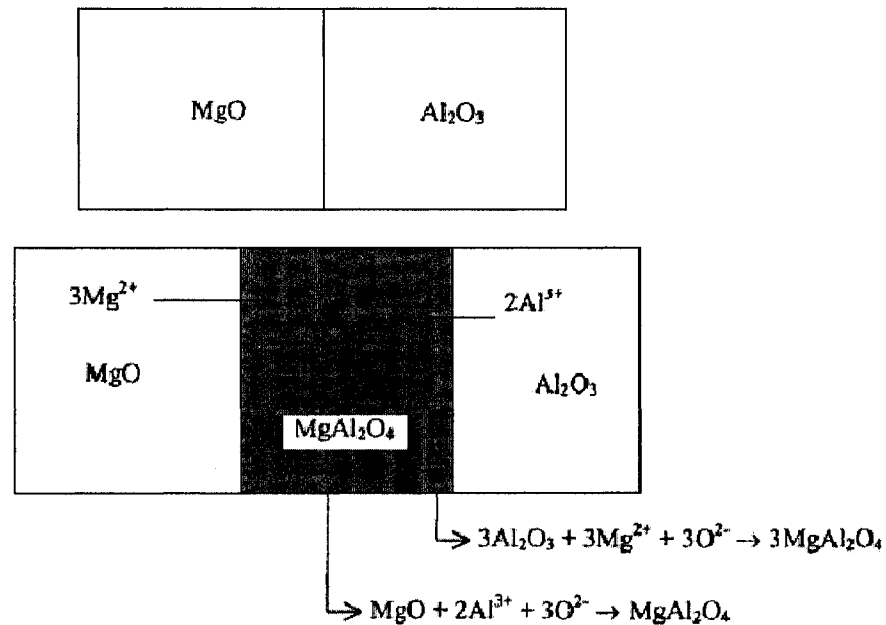
Figure 4.17: *Reaction mechanism and phase boundary reactions for spinel formation:*
$MgO + Al_2O_3 \rightarrow MgAl_2O_4$ [96]

The driving force for reaction is the difference in the Gibbs free energy between the reactants and product. The standard Gibbs free energy changes, $\Delta G°$, for the possible reactions are plotted in Figure 4-18 as a function of temperature. According to the values of driving forces, the reaction for spinel formation is less favorable than others due to its relatively lower Gibbs free energy. However, with increasing temperature it becomes more favorable due to more driving force reaction.

Figure 4-18 shows that formation of aluminum nitride and magnesium nitride is more favorable than MgO or spinel. Hence, in the experiments performed at 800, 950°C no un-reacted metal has been observed due to complete conversion of aluminum and magnesium vapor to aluminum nitride and magnesium nitride. Magnesium oxide is provided through magnesium reaction with the residual oxygen in the atmosphere and with alumina as can be seen in Equation 4-7. Therefore, the rate of MgO formation in the samples processed at 800 and 950°C is higher than that of samples at 650°C (Figures 4-6, 4-12, 4-16) due to oxidation of AlN.
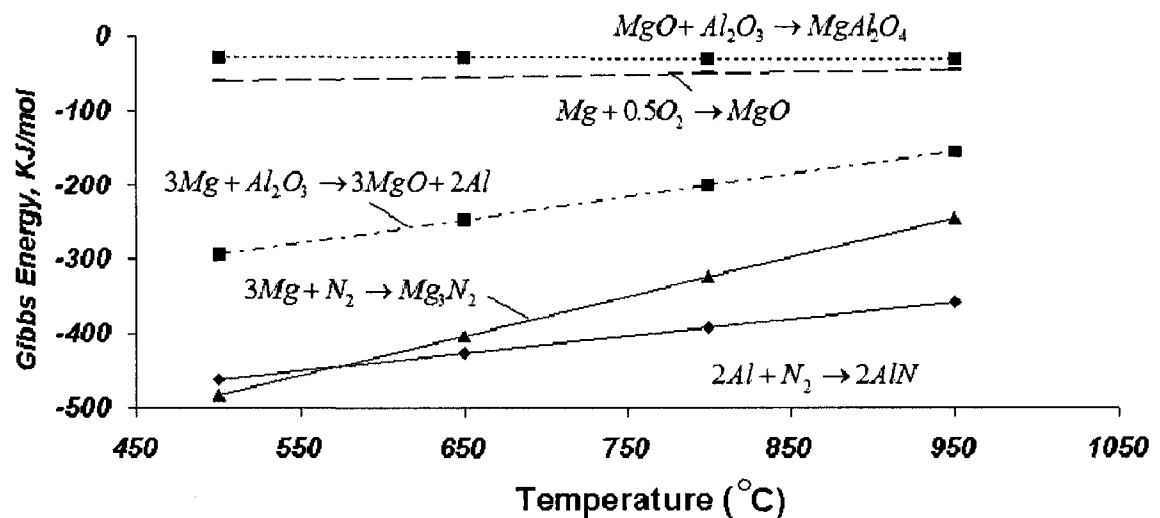
Figure 4.18: *Changes of standard Gibbs free energy with temperature*

The successful infiltration of magnesium into AlN performs can be explained according to the description by Kevorkijian [95], Hou [96], and Shtessel [109]. They proposed that when magnesium volatizes and reacts with oxygen and nitrogen, magnesium oxide and magnesium nitride form. Magnesium vapor is an active gas because of its high vapor pressure, as stated before. Then, magnesium nitride (Mg_3N_2) particles are formed first by reaction of vaporized magnesium and nitrogen gas. A thin

layer of Mg_3N_2 coats the surface of the aluminum nitride phase and improves spontaneous infiltration through significantly enhanced wetting. When magnesium nitride particles are introduced into molten aluminum a substitution reaction takes place between magnesium nitride and aluminum to form aluminum nitride (Figure 4-18). Hence, spontaneous infiltration in all samples was completed successfully.

In this work, the infiltration process was attempted with argon atmosphere at same holding temperatures and times, but products were fragile and infiltration was not successful. This proves that N_2 plays an important role as described in Fig. 4-19.
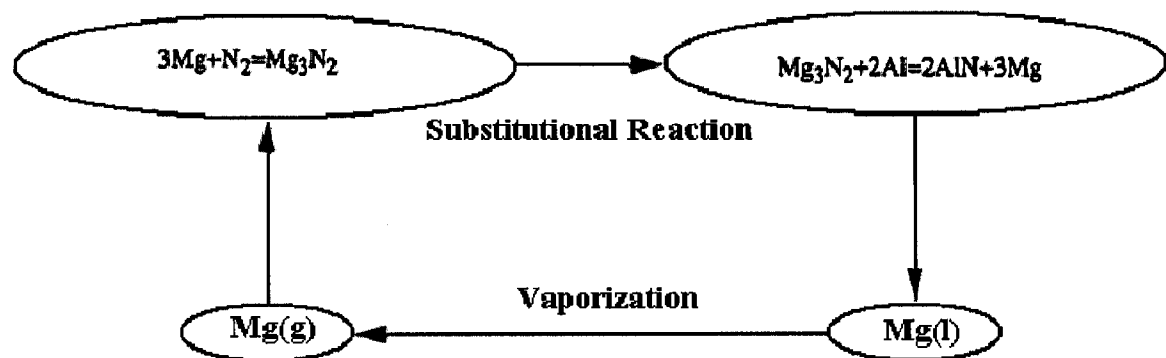
Figure 4.19: *Mechanism of magnesium nitride formation*

The needed molten aluminum to react with magnesium nitride was supplied from the magnesium alloy and as a product of the reaction between magnesium and alumina as follows:

$$Al_2O_3(s) + 3Mg(g) \rightarrow 2Al(l) + 3MgO(s) \qquad 4\text{-}7$$
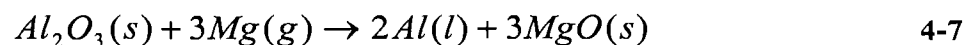
In samples processed at 650°C, molten aluminum is supplied only from the magnesium alloy (AZ91E), while in samples at 800, 950°C it is supplied from melting magnesium alloy and through reaction 4-7, because AlN oxidation, which provides

61

alumina to allow Equation 4-7 to proceed, takes place at higher than 750°C (Equation 4-6). Microstructures of samples show that small AlN particles with average 3-4 μm size, form at all holding temperatures (Figure 4-19). However, they were observed more in samples processed at 950°C rather than at lower temperatures. Hou [96] showed that formation of small AlN particles during nitridation of Al-Mg-Si alloys are due to substitutional reaction of Mg_3N_2 and molten aluminum.

Comparison of XRD patterns between AlN powder and products processed at 950°C and 135 min. show that Al_2O_3, which was earlier reported as almost 1.04 wt% in the AlN powder reduces to 0.85 wt%.
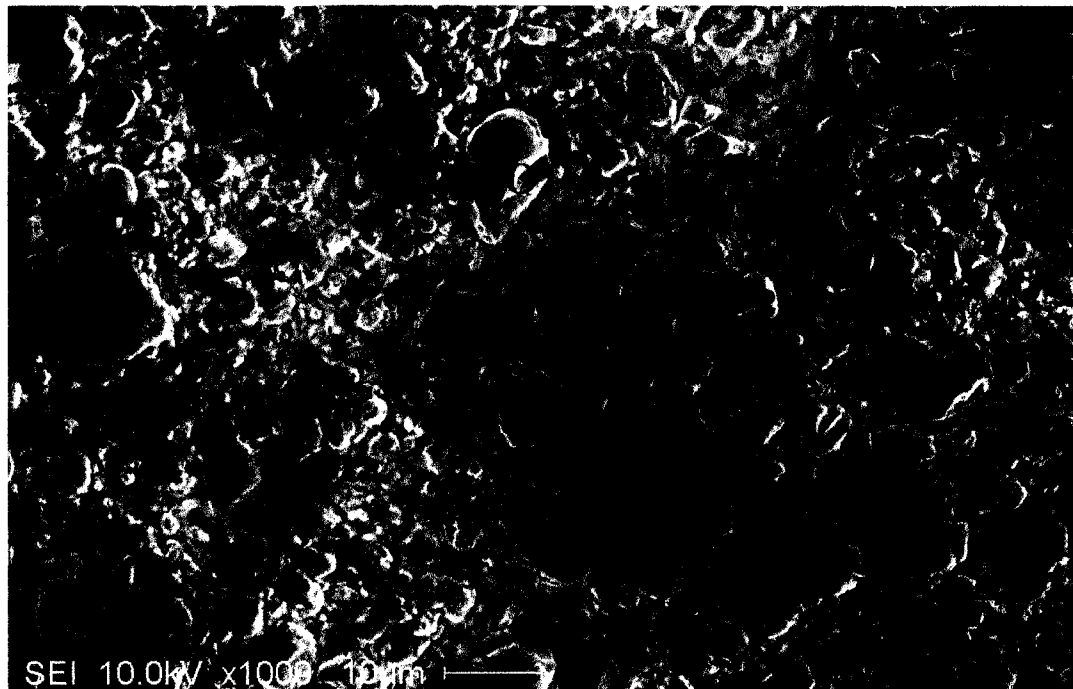
(a)
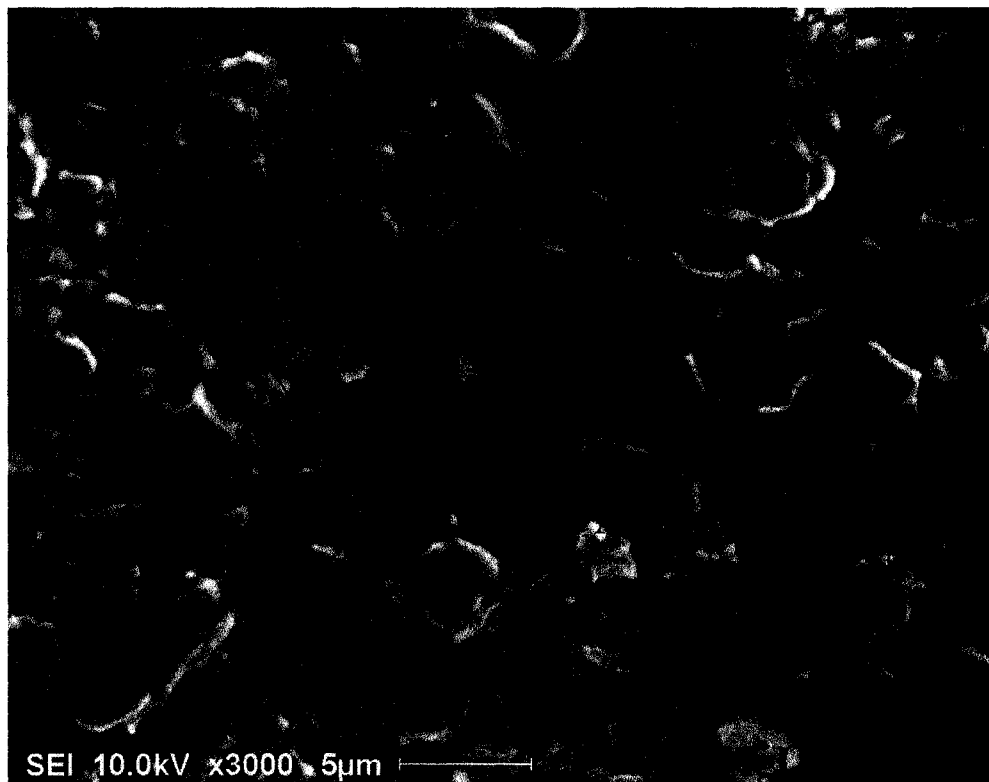
(b)
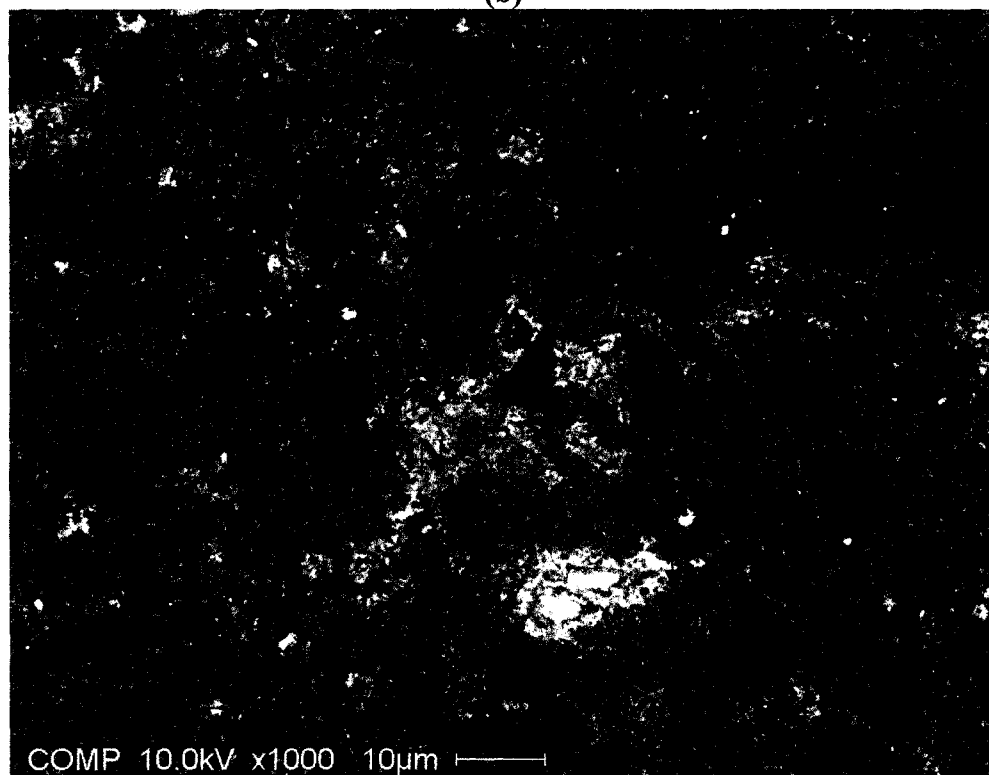
(c)

Figure 4-20: *Small particles in samples with a) 950 °C and 135 min. b) 800 , 25 min. c) 650 °C and 25 min.*

4.3 Physical properties

4.3.1 Density Measurement

The density of all samples was measured by Archimedes law, as described in chapter 4.3.1. The results are shown in Table 4.1. Theoretical density is estimated based on the rule of mixture as [24]:

$$\rho_c = \Sigma(f_i \times \rho_i) = f_1 \times \rho_1 + f_2 \times \rho_2 + \ldots + f_n \times \rho_n \qquad \textbf{4-10}$$

Where ρ_c is the density of the composite, ρ_i and f_i are the density and volume fraction of each constituent in the composite, respectively. Experimental porosity is measured according to ASTM standard C20-97 [102]. The differences between theoretical and experimental porosity is due to closed pores which were not taken into consideration. Bulk density was measured using the same standard.

    In the density values measured by Archimedes' method, some errors are generated from different specimen weight measurements; weight measurements of dry weight (D), suspended weight (S), and weight in air (W). The average error of dry, suspended, and air weights for 24 samples (two measurements were performed for each sample) are ± 0.09 %, ± 0.295 %, ± 1.58 %, respectively. The average error in the density measurement of samples is estimated as ± 1.60 %. All experiments were repeated and the average results are presented in Table 4-1.

Table 4.1: *Porosity Measurements*

Samples Processed at		Theoretical Porosity (%)	Experimental Porosity (%)	Bulk Density Measurements (g/cm³)	Relative Density (%)
Temp. (°C)	Time (min)				
650	25	15.28	14.99	1.897	64.67
650	60	14.97	14.68	1.998	68.11
650	90	14.674	14.39	2.004	68.31
650	135	14.061	13.74	2.104	71.72
800	25	21.441	19.32	1.498	51.06
800	60	16.114	14.52	1.998	68.11
800	90	15.137	13.64	2.135	72.78
800	135	14.937	13.46	2.159	73.60
950	25	23.333	20.1	1.447	49.32
950	60	15.522	13.97	2.058	70.15
950	90	14.322	12.89	2.198	74.93
950	135	12.888	11.6	2.451	83.55

Figure 4-21 shows the relationship between density and porosity. Figure 4-22 presents the effects of holding time and temperature on relative density, which was calculated from the ratio of bulk density and theoretical density.
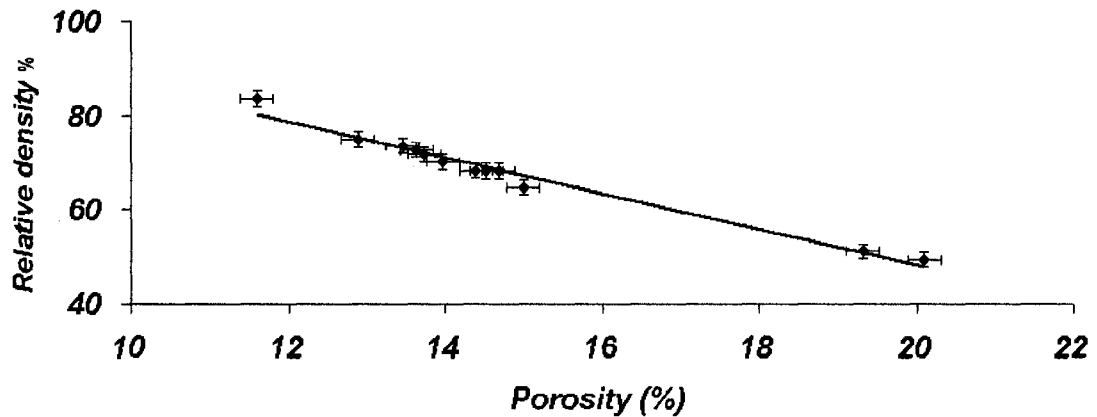
Figure 4.21: *The variation of density with porosity in all samples*
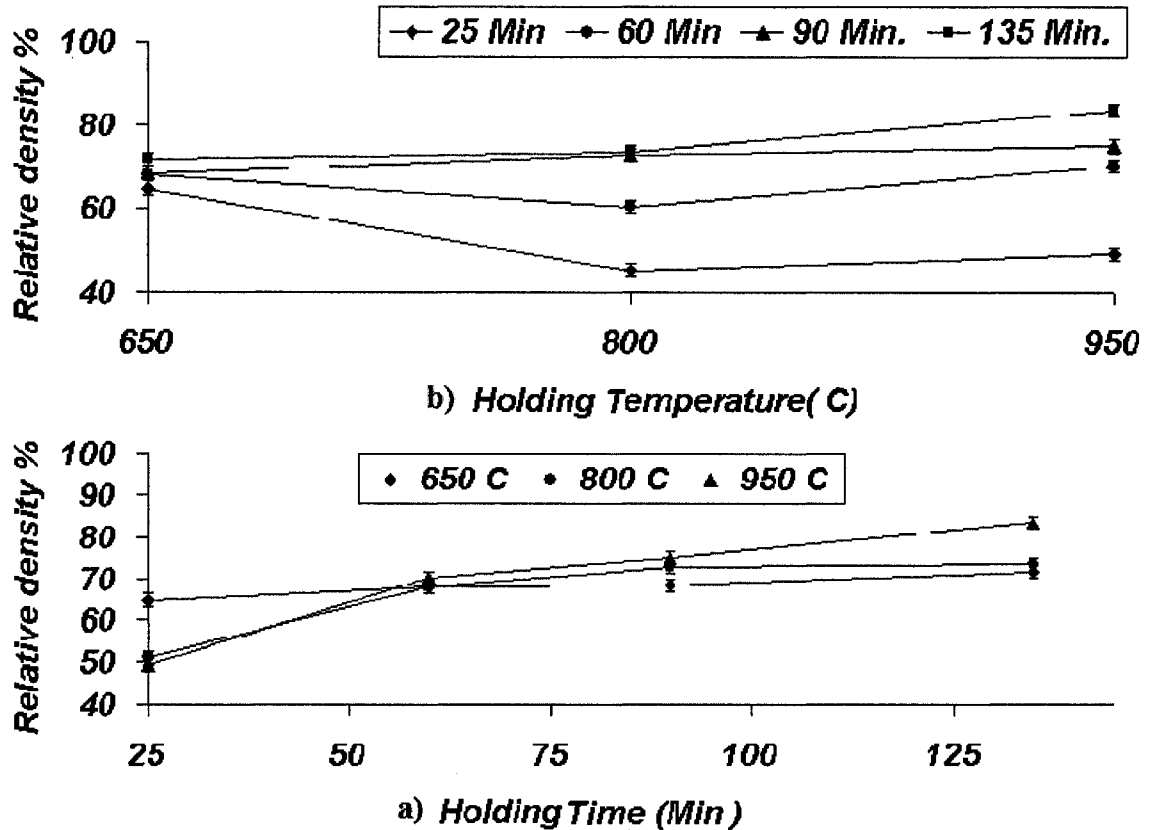
Figure 4.22: *The relative density versus: (a) Temperature (b) Times*

For holding times longer than 60 min, the relative bulk density increases with increasing temperature. Samples with less than 60 min holding time have more porosity and probably more gas inclusions due to insufficient time to fill the porous AlN preform. This is supported by Figure 4-22(b) which shows that increasing holding time resulted in higher density at all temperatures.

The reasons for the formation of porosity can be [107]:

- Incomplete infiltration of the molten metal,

- Gas inclusions which may form within the composites during the infiltration process, or

- Shrinkage due to solidification of molten metal.

Estimation of the amount of gas inclusions is difficult. However, the gas inclusion quantity depends on the direction of molten metal flow during infiltration and the process of solidification. Based on the principle of minimum resistance, the filling of spaces in porous AlN proceeds first with the largest capillaries and then as time passes, smaller and smaller capillaries.

4.3.2 Electrical Resistivity

Table 4.2 shows the results of bulk electrical resistivity. According to the manufacturer's recommendation samples were subjected to 500 volts and 2mA current. All samples processed at 650 °C holding temperature are conductors and those at 800°C and 950°C are insulators. The presence of metallic phases in the samples processed at 650 °C, of course, made them conductors.

Table 4.2: *Electrical resistance Measurements*

Samples Processed at		Bulk Electrical Resistivity of Samples (Ω.cm)	Bulk Electrical Resistivity of Replicas (Ω.cm)
Temp. (°C)	Time (min)		
650	25	Conductor	N/A
650	60	Conductor	N/A
650	90	Conductor	N/A
650	135	Conductor	N/A
800	25	6.73×10^9	1.19×10^{10}
800	60	5.73×10^{10}	9.98×10^9
800	90	1.44×10^{11}	2.65×10^{11}
800	135	2.27×10^{11}	3.98×10^{11}
950	25	1.42×10^{11}	9.8×10^9
950	60	1.85×10^{11}	1.85×10^{11}
950	90	2.04×10^{11}	3.45×10^{11}
950	135	2.10×10^{11}	6.58×10^{11}

Three measurements were performed for each sample and the average error was found to be ±0.09 %. The same measurements and error calculations for replicas were conducted and the average error of replicas estimated 0.12 %.

4.4 Thermal Properties

The two major properties related to heat conduction are thermal conductivity and thermal diffusivity. In this section, the main concern is calculating thermal conductivity of samples (800, 950°C) which are non-electrical conductors by measuring thermal diffusivity and heat capacity as described in Equation 3-3:

$$K = C_p \times \rho \times D$$

3-3

4.4.1 Thermal Diffusivity

Thermal diffusivity measurements were performed on samples as described in section 3.3.3. The thermal diffusivity values have been measured between 30-295°C (Figure 4-23). In all samples, thermal diffusivity decreased with increasing temperatures, but at different rates depending on the porosity content and bulk density. Figure 4-24 shows thermal diffusivity dependence on porosity and relative density of the samples processed at 800 °C and 950 °C. In samples with high density, thermal diffusivity increased because heat transfer across pores is ordinarily slow and inefficient.
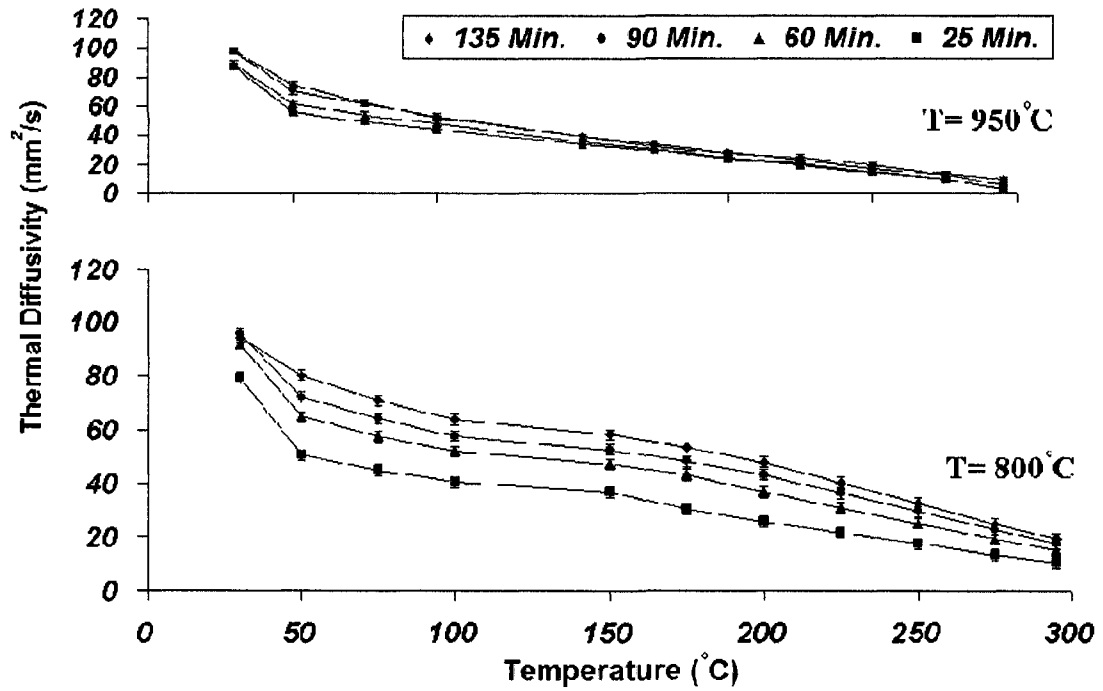
Figure 4.23: *Thermal diffusivity of samples processed at: (a) 950 °C (b) 800 °C*
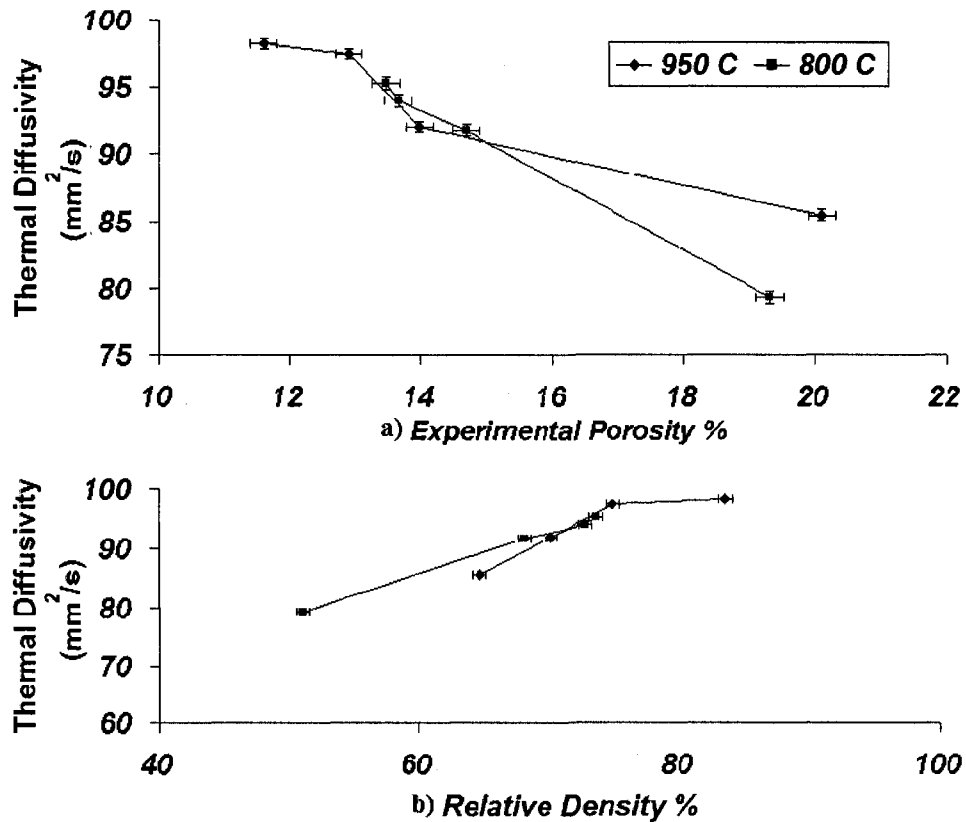
Figure 4.24: *Thermal diffusivity versus (a) porosity %, and (b) relative density % for 800°C and 950°C processing*

4.4.2 Heat Capacity

Measurement of heat capacity has been achieved by differential scanning calorimetery (DSC) between 30-295 °C. The measurement is made according to ASTM method E 1269 [108]. The results of this test are shown in Figure 4-25 and indicate that no decomposition or phase transformation during heating and cooling has occurred. Also, it is observed that the trend of heat flow for all holding times is similar and almost constant. Theoretically, Heat capacity can be calculated by the following equation:

$$C_p = (\frac{\partial H}{\partial T})_P \qquad\qquad\qquad \textbf{4-12}$$
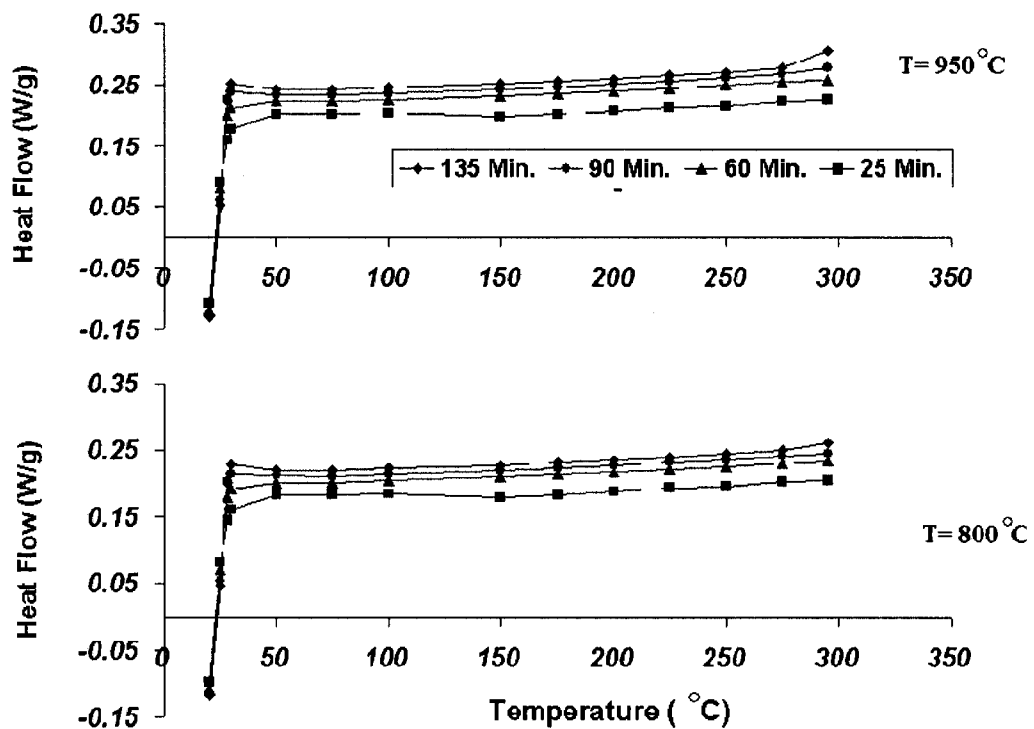
Figure 4-25: *Heat flow values between 30-295°C at 950°C and 800° C holding temperatures*

Variation of heat flow with temperature in the range of 30-295°C (Figure 4-25) can be considered as a linear relation, y=ax+b, and according to Equation 4-12, the

specific heat capacity is the slope of the line. Therefore, each sample has a constant value

of specific heat capacity as shown in Table 4-3.

Table 4.3: *Constant Values of C_p*

Samples Processed at		Specific Heat Capacity (J/g°C)
Temp. (°C)	Time (min)	
800	25	0.310
800	60	0.321
800	90	0.339
800	135	0.367
950	25	0.289
950	60	0.311
950	90	0.371
950	135	0.398

4.4.3 Thermal Conductivity

Based on the specific heat capacity and density values, thermal conductivity has

been plotted in Figure 4-26. The total error for the thermal conductivity was calculated as

±14 %. It is based on average error calculation of samples and replicas which are ±3.33%

and ±2.85%, respectively.

For the 950 °C and 135 min. condition, the maximum thermal conductivity value

of 95.88 W/m.K was achieved. With increased holding time, the density of the samples

increased resulting in enhanced thermal diffusivity and conductivity as can be seen in

Figure 4-27. The variation of thermal diffusivity and conductivity with porosity has been

plotted in Figure 4-28.
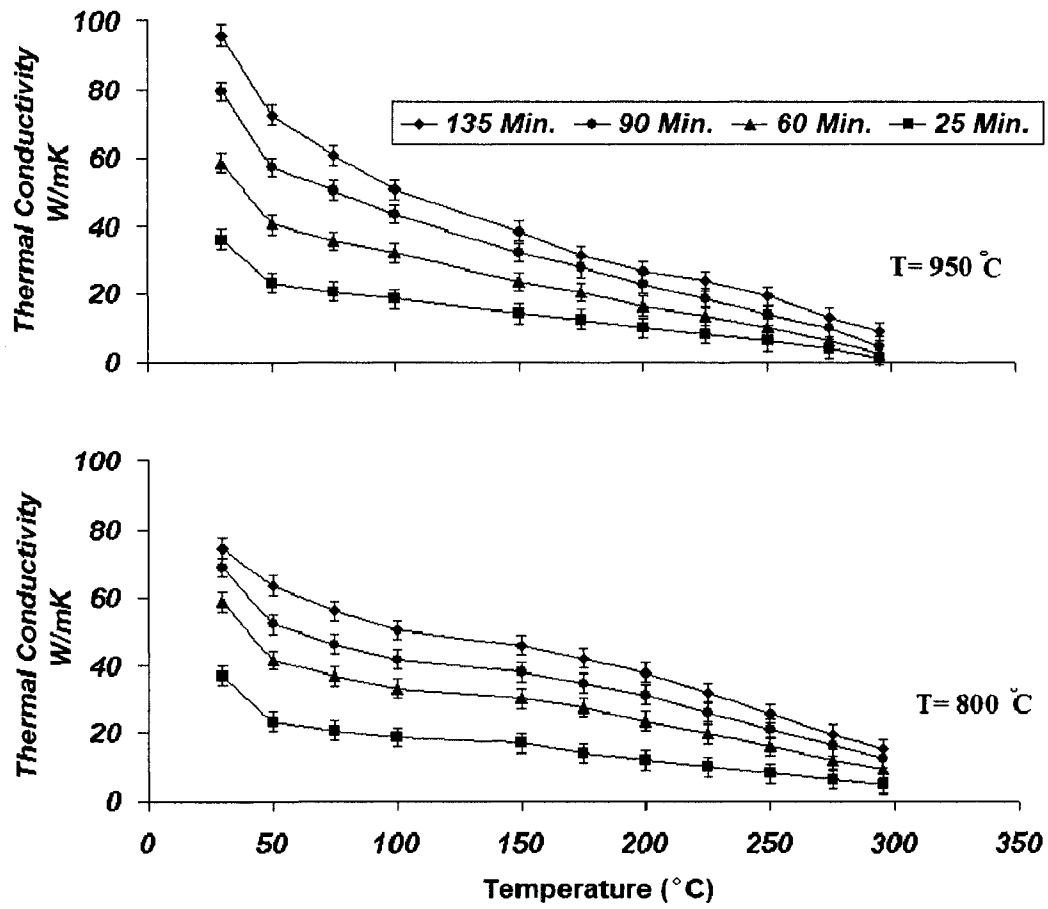
Figure 4-26: *Thermal conductivity versus temperature calculated with constant heat capacity*
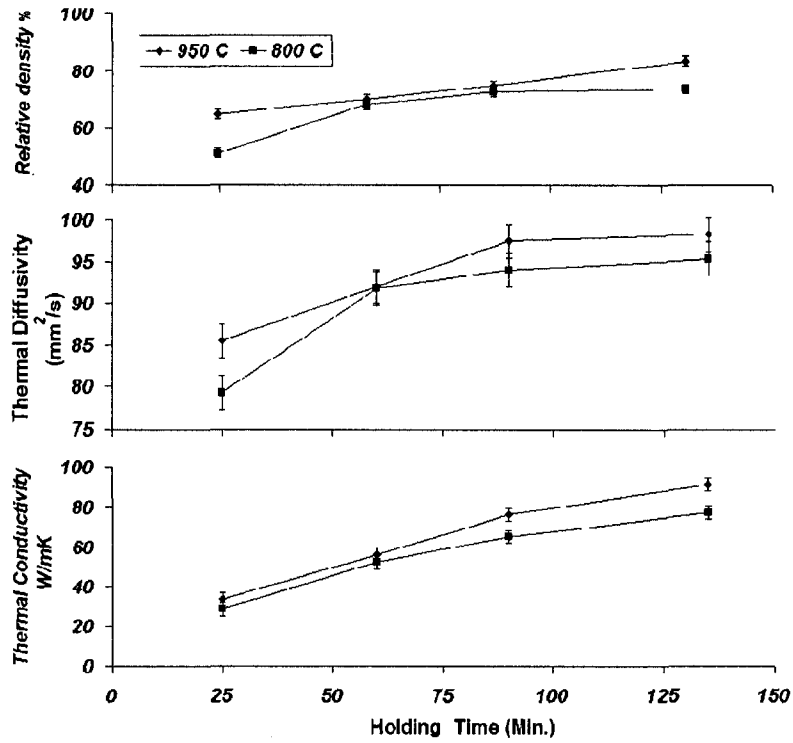
Figure 4-27: *Effects of density on thermal diffusivity and conductivity versus holding time at 800 °C and 950° C*
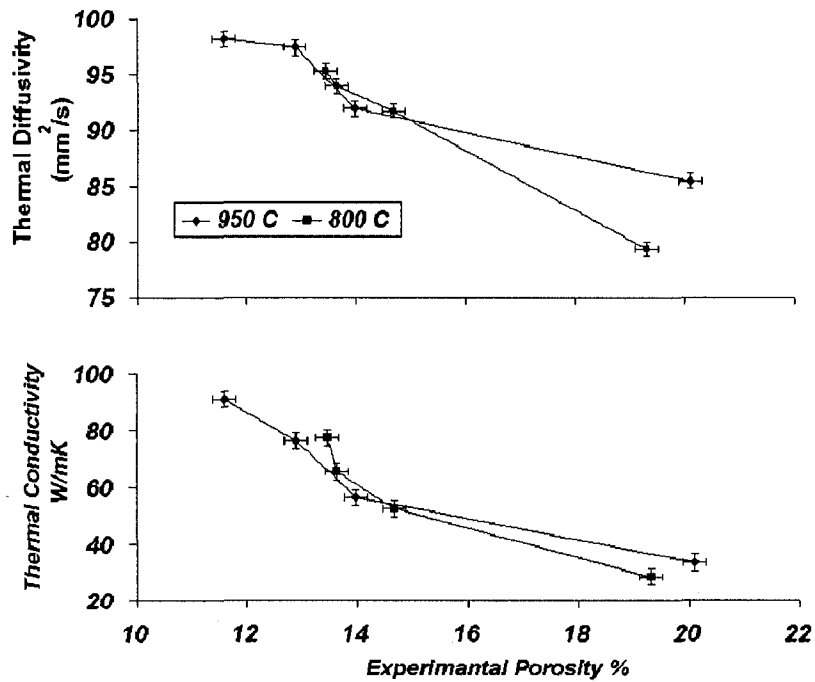
Figure 4-28: *Effect of porosity on thermal conductivity and diffusivity for 800°C and 950°C processing*

73

Table 4-4 shows a summary of all measurements and calculation. Electrically conducting samples (at 650 °C) were considered metal matrix composites which are not applicable as substrates and packages. Therefore, thermal properties have been calculated only for electrically insulating samples (800 °C, 950 °C).

Table 4-4: *Results of all measurements samples*

Sample	AlN/Mg Mass fraction (≈ 5/3)	Experimental Measurements		Resistance (Ω.cm) V= 500 V I= 2mA	XRD (Results)	Thermal diffusivity (mm²/s) @ 30 °C	Heat capacity (J/g °C) @ 30 °C	Thermal Conductivity (W/m.K) @ 30 °C	
		Porosity (%)	Bulk density (gr/cm³)					non constant Cp	constant Cp
T= 650 °C t= 25 min	6.15/3.8	14.99	1.897	Conductor	Al, Mg, MgO, AlN	------	------	Conductor	Conductor
T= 650 °C t= 60 min	5.16/3.11	14.68	1.998	Conductor	Al, Mg, MgO, AlN	------	------	Conductor	Conductor
T= 650 °C t= 90 min	3.98/2.40	14.93	2.004	Conductor	Al, Mg, MgO, AlN,$Mg_{17}Al_{12}$	------	------	Conductor	Conductor
T=650 °C T=135 min	11.224/7.01	13.74	2.104	Conductor	Al, Mg, MgO, AlN,$Mg_{17}Al_{12}$	------	------	Conductor	Conductor
T= 800 °C t= 25 min	5.46/3.36	19.32	1.498	$6.73 \times 10^{\wedge}9$	AlN, MgO	79.3	0.241	28.62	36.88
T= 800 °C t= 60 min	3.46/2.1	14.52	1.998	$5.73 \times 10^{\wedge}10$	AlN, MgO	91.76	0.285	52.25	58.85
T= 800 °C t= 90 min	4.87/2.89	13.64	2.135	$1.44 \times 10^{\wedge}11$	AlN, MgO	95.32	0.32	65.12	66.03
T=800 °C T=135 min	4.61/2.89	13.46	2.159	$2.27 \times 10^{\wedge}11$	AlN, MgO, Spinel	93.99	0.34	69.55	74.52
T= 950 °C t= 25 min	4.98/2.89	20.1	1.447	$1.42 \times 10^{\wedge}11$	AlN, MgO	86.47	0.268	33.53	36.19
T= 950 °C t= 60 min	5.23/3.3	13.97	2.058	$1.85 \times 10^{\wedge}11$	AlN, MgO	88.73	0.317	57.88	58.68
T= 950 °C t= 90 min	4.36/2.7	12.89	2.198	$2.04 \times 10^{\wedge}11$	AlN, MgO, Spinel	97.44	0.356	76.24	79.5
T=950 °C T=135 min	15.46/9.56	11.6	2.451	$2.10 \times 10^{\wedge}11$	AlN, MgO, Spinel	98.19	0.381	91.7	95.88

CHAPTER 5: CONCLUSIONS, CONTRIBUTIONS TO KNOWLWDGE, AND SUGGESTIONS FOR FUTURE WORK

5.1 Conclusions

Reactive pressureless infiltration is a common and low cost method to fabricate metal and ceramic matrix composites. Homogeneous distribution of matrix and reinforcing phase and near net-shape products are some advantages of this technique. However, controlling and monitoring reactions are difficult. The present research was carried out to investigate the fabrication of ceramic composites of non-sintered aluminum nitride using reactive spontaneous infiltration of molten magnesium alloy (AZ91E) into a porous preform of aluminum nitride powder in a nitrogen atmosphere. Magnesium alloy was selected due to its low melting temperature and high affinity for oxygen. Samples were examined and from the results the following conclusions can be drawn:

1. Full infiltration of molten magnesium into AlN preform under nitrogen gas takes place and samples fabricated at temperatures above 650°C were electrical insulators. However, for the same process with an argon atmosphere incomplete infiltration was observed. Furthermore, all samples in argon atmosphere were conductors.

2. A simple procedure to fabricate AlN/MgO and AlN/MgO, $MgAl_2O_4$ composites with in situ spontaneous infiltration was developed.

3. The pressureless infiltration occurs at relatively low temperature (650-950°C) in two directions, downward and upward simultaneously by using proper compaction of the AlN preform,

4. In the samples processed at 800°C and 950°C, ceramic matrix composites were obtained because the following reactions took place:

$$Al_2O_3(s) + 3Mg(g) \rightarrow 2Al(l) + 3MgO(s)$$

$$2Al(l) + N_2(g) \rightarrow 2AlN(s)$$

$$Mg_3N_2(s) + 2Al(l) \rightarrow 2AlN + 3Mg$$
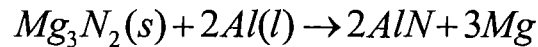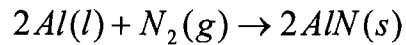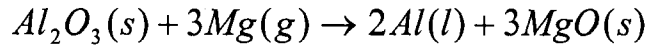
5. The proposed mechanism to complete infiltration is based on the formation of Mg_3N_2 phase, which completely or partially coats the AlN preform and enhances wetting.

6. The maximum thermal conductivity value, 95.88 W/m.K, was obtained for the sample processed at 950 °C and 135 min.

7. The effects of porosity have been investigated and revealed that it has drastic effects on thermal conductivity.

5.2 Contributions to knowledge

A novel ceramic matrix composite using non-sintered AlN was fabricated at low temperatures (650-950°C). A reasonable thermal conductivity (95.88 W/m.K) with a low cost method was achieved. This is the first attempt to explain the infiltration behavior and the corresponding thermal conductivity of non-sintered AlN using pressureless infiltration of magnesium alloy (AZ91E).

5.3 Suggestions for future work

Although the spontaneous infiltration was achieved, it is recommended that the effects of the following parameters be investigated:

- AlN particle size on thermal conductivity

- Using other gas such as a mixture of NH_3 and N_2 or N_2/H_2.

- Coating the AlN powder with a thin layer of magnesium, to control porosity and density of products

- Using a Mg alloy composition with a different Al/Mg ratio, to achieve the best thermal conductivity

REFERENCES

1. B. Dinwiddie," *Thermal Conductivity of Materials for Electronic Packaging Substrates*" PhD thesis, University of Delaware, USA, 1991

2. B. Dinwiddie, A. Whittaker, and D. Onn, "*Thermal Conductivity, Heat Capacity, and Thermal Diffusivity of Selected Commercial AlN substrates*" International Journal of Thermophysics,Vol.10,No.5,1989,pp.1075-1084

3. N. Chawla and K.K Chawla, *"Metal Matrix Composites*" Springer Science and Business Media, Inc. USA, 2006

4. A. Virkar, T. Jackson and R. Cutler, "*Thermodynamic and Kinetic Effects of Oxygen Removal on the Thermal Conductivity of Aluminum Nitride*", Journal of American Ceramic Society,Vol.72,No.11,1989,pp.2031-42

5. M. Borom, G. Slack, and J. Szymaszek, "*Thermal Conductivity of Commercial Aluminum Nitride*", American Ceramic Society Bulletin,Vol.51,No.11,1972,pp. 852-56

6. G. Slack, R. Tanzilli, R. Pohl, and J. Vandersande, "*The Intrinsic Thermal Conductivity of AlN* ", Journal of Physics Chemistry Solids,Vol.48,No.7,1987,pp. 641-47

7. G. Slack, "*Nonmetallic Crystals with High Thermal Conductivity*", Journal of Physics Chemistry Solids,Vol.34,1973,pp.321-35

8. J. Nipko and C. Loong, "*Phonon Excitations and Related Thermal Properties of Aluminum Nitride*" Physic Review Bulletin,Vol.57,No.17,1989,pp.10550-554

9. F. Miyashiro, N. Iwase, A. Tsuge, F. Ueno, M. Nakahashi and T. Takahashi, "*High Thermal Conductivity Aluminum Nitride Ceramic Substrates and Packages*", IEEE Transactions on Composites, Hybrids, and Manufacturing Technology,Vol.13,No.2,1990,pp.313-319

10. Y. Baik, R. Drew "*Aluminum Nitride: Processing and applications*", Key Engineering Materials,Vols.122-124,1996,pp.553-570

11. N. Kuramoto, H. Taniguchi and I. Aso, "*Development of Translucent Aluminum Nitride Ceramics*", American Ceramic Society Bulletin,Vol.68,1989,p.886

12. A. Hafidi, M. Billy, J. Lecompte, "*Influence of Microstructural Parameters on Thermal Diffusivity of Aluminum Nitride-Base Ceramics*", Journal of Materials Science,Vol.27,1992,pp.3405-3408

13. L. Sheppard, "*Aluminum Nitride: A Versatile but Challenging material*", Ceramic Bulletin,Vol.96,No.11,1990,pp.1801-1812

14. Y. Baik, "*Sintering of Aluminum Nitride with Y_2O_3 by Secondary Phase Composition Control*", PhD thesis, McGill University, Canada, 1995

15. B. Modrike and T. Ebert, "*Magnesium properties-applications-potential*" Material Science and Engineering A,Vol.302,No.1,2001,pp.37-45

16. A. Luo, *"Processing, Microstructure, and Mechanical Behavior of Cast Magnesium Metal Matrix Composite"*, Metallurgical Material Trans. A,Vol.26A,1995, p.2445

17. K. Wu, M. Zheng, M. Zhao, C. Yao, and J. Li, *"Interfacial Reaction In Squeeze cast SiCw/AZ91 Magnesium Alloy Composite"*, Scripta Materiallia,Vol.35, No.4,1996,pp.529-34

18. *M. Zarinejad, S. Firrozi, P. Abachi, K. Purazrang, "The Effect of Reinforcement Parameters and Aging Heat Treatment on The Mechanical Properties of Magnesium Matrix AZ91-SiC Composites"* Proceeding of 41st Conference of Metallurgists of Canadian Institute of Mining, Metallurgy and Petroleum, Metal/Ceramic Interactions, Montreal, Quebec, Canada 2002,pp.191-203

19. X. Zhang, *"Squeeze Casting of Magnesium Matrix Composites Reinforced With Alumina Short Fibers"*, Master of Engineering Project, McGill University, Canada, 2004

20. O. Ottinger, C. Grau, R. Winter, R. Singer, A. Feldhoff, E. Pippel and J. Woltersdorf , *"The effect of Aluminum Additions on the Interfacial Microstructure and Mechanical Properties of Mg Composites"* Proceeding of ICCM10; Woodhead Publishing Ltd., Cambridge.Vol.VI,1995,pp.447-454

21. C. Leon, Y. Arroyo, E. Bedolla, E. Aguilar and R. Drew, *"Properties of AlN-Based Magnesium Matrix Composites Produced by Pressureless Infiltration"*, Material Science Forum,Vol.509,2006,pp.105-110

22. Y. Arroyo, V. Lopez, E. Aguilar and E. Bedolla, *"Processing of Mg/AlN Composites by Pressureless Infiltration"*, Proceedings of Com.2002, Metal/Ceramics Interaction, Montreal, Canada,2002 ,pp.205-215

23. W. Callister, *"Materials Science and Engineering: An Introduction"*, John Wiley and sons Inc. Sixth edition, USA, 2003

24. D. Askeland, P. Phule, *"The Science and Engineering of Materials"*, Thomson Inc., Fifth edition, USA, 2006

25. E. Degarmo, J. Black, R. Kohser, *"Materials and Processing in Manufacturing"*, John Wiley and Sons Inc. Ninth Edition, USA, 2003

26. M. Medraj, *"Phase Equilibria in The AlN-Al2O3-Y2O3 System - Utility AlN Processing"*, PhD thesis, McGill University, Canada, 2001

27. A. Junior, D. Shanafield, *"Thermal Conductivity of Polycrystalline Aluminum Nitride (AlN) Ceramics"* Ceramica,Vol.50,2004,pp.247-253

28. L. Pauling, *"The Nature of Chemical Bonding"*, Cornell University Press, Thaca,NY,1960,pp.64-107

29. P. Baranda, A. Kundsen and E. Ruh," *Effect of silica on the thermal conductivity of Aluminum Nitride"*, Journal of American Ceramic Society,Vol.76,No.7,1993,pp.1761-1771

30. W. Kingery, H. Bowen and D. Uhlam, *"Introduction to Ceramics"*, John Wiley and sons Inc. NY,1976

31. D. Richerson, *"Modern Ceramic Engineering"* Marcel Dekker Inc.,1982,p.136

32. A. Eucken, *"On The Temperature Dependence of The Thermal Conductivity Of Several Gases"*, physic Z.Vol.12,1911,p.1005

33. P. Debye, *"Interference of Röntgen rays heat Motions"*, Annual Physic,1914, Leipzig,p.46

34. R. Berman, F. Simon, and J. Wilks, *"Thermal Conductivity of Dielectric Crystals"*,Nature,Vol.168,1951,pp.277-280

35. N. Iwase, A. Tsuage, and Y.Sugiura, *"Development of high thermal conductive aluminum nitride ceramic substrate technology"* proceeding of the 3rd, international microelectronics conference,1984,pp.180-185

36. H. Nakao, K. Watari, H. Hayashi, K. Urabe ,*"Microstructural Characterization of High Thermal Conductivity AlN Ceramic"*, Journal of American Ceramic Society Vol.85,No.12,2002,pp.3093-95

37. M. Kasori & F. Ueno, *"Thermal conductivity Improvement of YAG added Aluminum nitride ceramics in the grain boundary elimination process"* Journal of The European Ceramic Society,Vol.15,1995,pp.435-443

38. Y. Kurokawa, K. Utsomi, H. Takamizawa, T. Kamata, and S. Noguchi, *"AlN substrates with high thermal conductivity"*, IEEE Transactions on Components, Hybrids, and Manufacturing Technology,Vol.chmt-8,No.2,June 1985

39. T. Okada, M. Turiyama, and S. Kanazaki *"Synthesis of AlN sintered bodies using the direct nitridation of Al compacts"*, Journal of European Ceramic Society,Vol.20,Issue 6,May 2000,pp.783-787

40. P. Baranda, A. Kundsen and E. Ruh," *Effect of CaO on the thermal conductivity of Aluminum Nitride"*, Journal of American Ceramic Society,Vol.76,No.7,1993, pp.1751-1760

41. G. Long and , L. Foster, *"Aluminum Nitride, a Refractory for Aluminum to 2000° C "*, Journal of American Ceramic Society,Vol.42,No.2,1959,p.53

42. G. Slack, T. McNelly, *"Growth of high purity AlN crystals"*, Crystal Growth Journal,Vol.34,1976,pp.263-279

43. A. Abid, R. Rensalem, and B. Sealy, *"The thermal stability of AlN"*, Journal of Materials Science,Vol.21,1986,pp.1301-1304

44. I. Dutta, S. Mitra, and L. Rabenberg, *"Oxidation of sintered aluminum nitride at near-ambient temperatures"* Journal of American Ceramic Society,Vol.75,No.11, 1992,pp.3149-53

45. K. Taylor and C. Lenie, *"Some properties of AlN"*, Journal of Electrochemical International,Vol.4,1991,pp.879-882

46. A. Maghsoudipour, F. Moztarzadeh, M. Saremi, and J.G. Heinrich *"Oxidation behavior of AlN-Al₂O₃ composites"* Ceramics International ,Vol.30,Issue 5,2004,pp.773-783

47. R. Buchanan,*"Ceramic materials for electronics"*, Marcel Dekker, Inc. New York, USA, 1986

48. N. Kim, K. Komeyand, T. Meguro, *"Effect of Al₂O₃ addition on phase relation of AlN-Y₂O₃ system"* Journal of Materials Science,Vol.31,No.6,2000,pp.1603-1608

49. J. Schuster, *"Phase Diagram Relevant for Sintering Aluminum Nitride Based Ceramics"*, Revue de Chimie Mineral, Vol.24,1987,pp.676-686

50. K. Watari, M. Kawamoto, and K. Ishizaki, *"Sintering Chemical Reaction to Increase Thermal Conductivity of Aluminum Nitride"*, Journal of Materials Science,Vol.26,1991,pp.4727-4732

51. T. Troczynski and P. Nicolson, *"Effect of Additives on The Pressureless Sintering of Aluminum Nitride Between 1500 °C and 1800 °C"* Journal of American Ceramic Society,Vol.72,No.8,1989,pp.1488-1491

52. K. Watari, H. Hwang, M. Toriyama, S. Kanazaki, *"Effective sintering aids for low temperature sintering of AlN ceramics"* Journal of Material Research,Vol.14,No. 4,Apr.1999

53. A. Junior, D. Shanfield, *"The use of yttrium III isopropoxide to improve thermal conductivity of polycrystalline aluminum nitride (AlN) ceramics"* Journal of Materials Science: Materials in Electronics,Vol.16,2005,pp.139-144

54. K. Shinzoke, M. Kasori, K. Anzari, H. Inoue, and A. Tsuage, *"AlN ceramic with high thermal conductivity; 3.Effects of additives on thermal conductivity"*, Presented at American Conference Ceramic Society, Japan, May 1985

55. Spark Plug Co. Ltd Website, *"AlN ceramic package/substrate"* Communication Media Components Group, Sept 2002, www.ntktech.com/AlN

56. Z. Xin, L. Yawei, J. Sheng, L. Nan, Z. Jiuxing, *"Preparation of MgO/AlN Composites by melt infiltration process"* Journal of the Chinese Ceramic Society,Vol.32,No.9,2004,pp.1078-1081

57. M. Kuntz, S. Diekes, and G. Grathwhol, *"Reaction Sintering for the Production of MgAl₂O₄-Spinel-Based Composite Ceramics"* Journal of American Ceramic Society,Vol.88,No.3,pp.553-559

58. A. Kelly, *"Composites materials after seventy years"*, Journal of Materials Science,Vol.41,2006,pp.905-912

59. D. Kopeliovich, SubsTech. (Substances&Technologies) website, http://www.substech.com , April 2007

60. H. Ye, X. Liu, *"Review of recent studies in magnesium composites"* Journal of Materials Science,Vol.39,2004,pp.6153-6171

61. R. Saravanan and M. Surappa, *"Fabrication and characterisation of pure magnesium-30 vol.% SiC particle composite"* Material Science Engineering A Vol.276,2000,p.108

62. S. Lim and T. Choh, *"Effect of Alloying Elements on SiC Particulate Dispersion Behavior in Molten Magnesium"*, Journal of Japanese Industrial Metallurgy,Vol.56,No.9,1992,p.1101

63. N. Harnby, M. Edwards and A. Nienow, *"Mixing in process Industries"* Butter worths Series Ltd. London,1985

64. S. Ray, *"Synthesis of Cast Metal Matrix Particulate Composites"*, Mtech Dissertation, Indian Institute of Technology, Kanpur,1969

65. A. Mortenson and J. Cornie, *"On The Infiltration Of Metal Matrix Composites"*, Metallurgical and Materials Transaction A,Vol.18A,1987,p.1160

66. V. Michaud and A. Mortenson , *"Infiltration of Fiber Preforms by a Binary Alloy"* Metallurgical and Materials Transaction A,Vol.23A,1992,p.2281

67. K. Wu, M. Zheng, C. Yao, S. Tatsuo, T. Hiroyasu, K. Akihiko and D.Li, *"Crystallographic Orientation relationship between SiCw and Mg in Squeeae-cast SiCw/Mg Composites"*, Journal of Material Science Letters,Vol.18,No.16,1999,pp.1301-1303

68. K. Wu, M. Zheng, M. Zhao, C. Yao, and J.Li, *"Interfacial reaction in squeeze cast SiCw/AZ91 magnesium alloy composite"*, Scripta Materialia,Vol.35,Issue 4,1996,pp.529-534

69. L.Hu and E. Wang, *"Fabrication and mechanical properties of SiCw/ZK51A magnesium matrix composite by two-step squeeze casting"*, Material Science and Engineering A,Vol.278,2000,pp.267-271

70. K. Dhingra, *"Aluminum Fiber FP"*, Philosophical Transactions of the Royal Society of London. Series A, Mathematical and Physical Sciences,Vol.294,Issue 1411,pp.411-416

71. H. Westengen, D. Albright , A. Nygard, Society of Automotive Engineering Technical Paper Number 900534, Society of Automotive Engineering, Detroit, Michigan,pp.606-616

72. M. Aghajanian, M. Rocazella, J. Burke, S. Keck, *"The infiltration of metal matrix composites by a pressureless infiltration technique"*, Journal of Materials Science, Vol.26,1991,pp.447-454

73. M. Aghajanian , J. Biel, and R. Smith, *"AlN matrix composites fabricated via an infiltration and reaction approach"* Journal of American Ceramic Society,Vol.77 No.7,1994,pp.1917-20

74. H. Kaneda and T. Choh, *"Fabrication of particulate reinforced magnesium composites by applying a spontaneous infiltration phenomenon"* Journal of Materials Science,Vol.32,1997,pp.47-56

75. R. Asthana, P. Rohatgi, and S. Tewari, *"Infiltration Processing of Metal Matrix Composites: A Review"*, Processing of Advanced Materials,Vol.2,1992,pp.1-17

76. D. Muscat and R. Drew, *"A method of measuring metal infiltration rates in porous performs at high temperature"* Journal of Material Science Letters,Vol.12,1993,pp.1567-1569

77. H. Chen, *"Fabrication of Magnesium Matrix Composites Using a Spontaneous Infiltration Technique"*, Master of Engineering Thesis, McGill University, Canada,Nov. 2002

78. T. Ebert, F. Moll, and K. Kainer, *"Spray Forming of Magnesium Alloys and Composites"*, Powder Metallurgy,Vol.40,Issue 2,1997,pp.126-130

79. P. Vervoort and J. Duszczyk , *"Technology of Magnesium and Magnesium Alloys"*, MPR publishing service Ltd.,UK,1992,p.13

80. A. Noguchi, I. Ezawa, J. Kaneko, and M. Sugamata, *"SiCp/Mg-Ce and Mg-Ca Alloy Composites Obtained by Spray Forming"*, Journal of Japanese Institute Light Metal,Vol.45,No.2,1995,p.64

81. K. Lee, H. Sim, H. Kwon, *"Fabrication pf Al/AlN composites by insitu reaction"*, Journal of Materials Science,Vol.41,2006,pp.6347-6352

82. C. Zhang, W. Cao, T. Fan, D. Zhang, *"Fabrication and formation mechanism of insitu AlN and Mg2Si particles-reinforced Mg matrix composites"*, Key Engineering Materials,Vol.351,2007,pp.151-155

83. R. Labotz and D. Mason, *"The Thermal Conductivities of Mg2Si And Mg2Ge"* Journal of Electrochemistery Society,Vol.110,1963,p.121

84. C. Takao, K. Makoto, N. Hiromichi and K, Hiromitu, *"Fabrication of metal matrix composite by spontaneous in filtration and subsequent in situ reaction processes"* Material Science Forum,Vol.353,1996,pp.217-222

85. K. Yamada, T. Takahashi, and M. Motoyama, *"EPMA State Analysis of Formation of TiC During Mechanical Alloying of Mg, Ti and Graphite Powder Mixture"* Journal of The Japan Institute of Metals,Vol.60,No.1,1996,p.100

86. K. Chawala, *"Ceramic matrix Composites"* Kluwar Academic Publisher, Massachusetts, USA, 2003

87. L. Lu, B. Chua, and M. Lai, *"Influence of SiC Particles on Mechanical Properties of Mg based Composites"* Composite Structure,Vol.47,1999,pp.595-601

88. A. Yamazaki, J. Kaneko, and M. Suganmata, J. Jpn. Soc. Powder Metall. (Japan) 48 (10) (2001) 935

89. H. Sreckert, K. Norton, and C. Wong, *"Hermetic SiC Composite Tubes"* American Ceramic Society Bulletin,Vol.75,No.12,1996, pp.61-64

90. T. Watari, S. Shimomura, T. Torikai and Y. Imaoka, *"Reactive infiltration of magnesium vapor into aluminum compacts"*, Journal of European Ceramic Society,Vol.19,Issue 10,August 1999,pp.1889-1893

91. W. Hillig, R. Mehan, C. Merelock, V. DeCarlo and W. Laskow, '*Silicon/silicon carbide composites*" American Ceramic Society Bulletin,Vol.54,No.12,1975,p. 1054

92. M. Newkirk, H. Zwicker, and A. Urquhert, "*Composite Ceramic Articles and Methods of Making the Same*", European Patent Applications, No. 86300739-9, Publ. No.0193292 Filed 04.02.86

93. M. Newkirk, A. Urquhert, H. Zwicker, and E. Breval, "*Formation of Lanxide Ceramic Composites Materials*", Journal of Materials Research,Vol.1,No.1, 1986,pp.81-89

94. M. Gurmazi, "*SiC Reinforcing Al₂O₃/Metal Composites by Direct Metal Oxidation*", PhD thesis, McGill University, Canada, 1996

95. V. Kevorkijian, T. Kesmak, K. Kiristoffer, "*Spontaneous Reactive Infiltration of Porous Ceramic Preforms with Al-Mg and Mg in the presence of both magnesium and nitrogen-new experimental evidence*" Materials and Manufacturing Processes,Vol.17,No.3,2002,pp.307-322

96. Q. Hou, R. Mutharasan, M. Koczak, "*Feasibility of AlN Formation in Aluminum Alloys*" Material Science Engineering A,Vol.195A,1995,pp.121-129

97. F. Duncan, "*Expansion During The Formation Of The Magnesium Aluminum Spinel (MgAl₂O₄) From Its Basic Oxide (MgO And Al₂O₃) Powders*" PhD thesis, University of Alabama, USA, 2004

98. H. Scholz and P. Greil, "*Nitridation reactions of molten Al-(Mg, Si) alloys*" Journal of Materials Science,Vol. 26,No.3,1991,pp.669-677

99. B. Rao and V. Jayaram, "*The Initiation and Continuation of Infiltration of Al-Mg Based Alloys Into Alumina Preforms*", Proceeding of the 3rd PRICM Conference on Advanced Materials and Processing,1988,pp.367-372

100. N. Nagendra, B. Rao and J. Jayaram, "*Microstructures and Properties of Al₂O₃/Al-AlN Composites by Pressureless Infiltration of Al-Alloys*" Materials Science and Engineering A,Vol.269,1999,pp.26-37

101. M. Aljarah, "Thermodynamic Modeling and Experimental Investigation of the Mg-Al-Ca-Sr system", PhD thesis, Concordia university, Canada, 2008

102. ASTM standard C20-73, "*Standard Test Methods for Apparent Porosity, Water Absorbtion, Apparent Specific Gravity, and Bulk Density of Burned Refractory Brick and Shapes by Boiling Water*" April 2000

103. G. Elssner, H. Horen, G. Kiessler, P. Wellner, "*Ceramic and Composites: Materialographic Preparation*", Elsevier Science Inc. NY.10010, USA, 1999

104. Pearson's Handbook, "*Crystallographic data for intermetallic phases*" Material Park, OH, 1997

105. C. Wagner, Z. Anorg, "*Mechanism of Counterdiffusion Through Reaction In The Solid State*". Allg. Chemistry,Vol.236,1938,pp.320-38

106. R. Carter, *"Mechanism of Solid State Reaction Between MgO and Al$_2$O$_3$ and Between MgO And Ferric Oxide"* Journal of American Ceramic Society, Vol.44, No.11, 1961, pp.116-120

107. J. Jackowski and J. Grabian, *"Porosity of Metal Infiltrated Composites- An Attempt At The Problem Analysis"*, Science and Engineering of Composite Materials, Vol.9, No.1, 2000, pp.17-24

108. TAinstrument Watters LLC, *"Thermal Specialty Library"*, Getting Started Guide, www.TAinstrument.com

109. V. Shtessel, *"Reactive Pressureless Infiltration Techniques for Cu-alloy/TiB2 and Other In-situ Composites: Processing, Modeling and Analysis"* PhD thesis, Drexel University, USA,1996

110. B. Hallstedt, *"Thermodynamic Assessment of the system MgO-Al$_2$O$_3$"* Journal of American Ceramic Society, Vol.75,No.6,1992, pp.1497-1507

APPENDIX A:

Thermal diffusivity is determined by subjecting the front face of a small disk test sample to a short pulse of light energy while recording the resulting temperature rise at the back face of the sample.
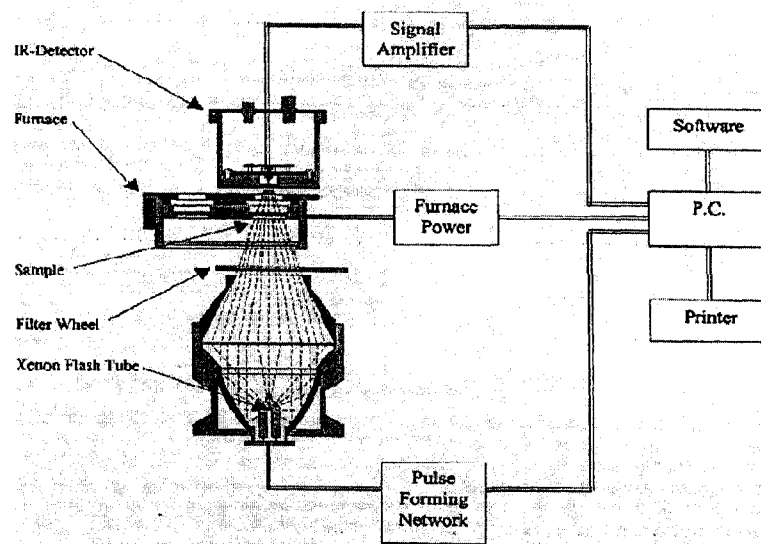
Figure A-1: LFA 447 Nanoflash Measuring Principl.

The back face temperature rise is measured during the test. Thermal diffusivity can be determined by comparing the measured data with the appropriate mathematic model such as, Parker, Cowan analysis, Koski procedure, and Taylor method. Cowan analysis has been recommended for ceramic materials by the laser flash equipment manufacturer. In this analysis, it was assumed that the energy pulse was rectangular in shape and of relatively short duration (Pulse time $t_p \ll t_{50}$). Cowan's theoretical relationships are:

$$ R = \frac{\theta_{5(t50)}}{\theta_{t50}} \quad \text{And} \quad C = \frac{\alpha t_{50}}{d^2} \qquad \text{A-1} $$
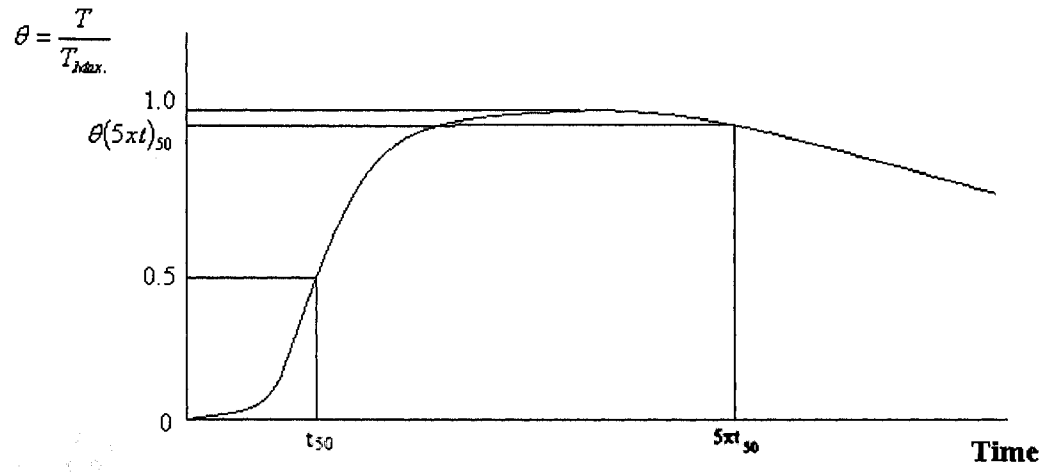
Figure A-2: *Cowan analysis curve*

APPENDIX B:

FactSage program with F.A.C.T data base has been used to predict heat capacity of samples. Proper conformity was found between modeling and measurements in samples with two phases, including MgO and AlN, up to 50 °C.

Samples	Heat Capacity J/g °C @ 30 °C			Phases
	Measurements	constant Heat Capacity Calculation	FactSage Modeling	
T= 800 °C t= 25 min	0.241	0.310	0.3098	AlN,MgO
T= 800 °C t= 60 min	0.285	0.321	0.2998	AlN,MgO
T= 800 °C t= 90 min	0.32	0.339	0.329	AlN,MgO
T=800 °C T=135 min	0.34	0.367	0.726	AlN,MgO,MgAl2O4
T= 950 °C t= 25 min	0.268	0.2893	0.278	AlN,MgO
T= 950 °C t= 60 min	0.317	0.311	0.315	AlN,MgO
T= 950 °C t= 90 min	0.356	0.371	0.898	AlN,MgO,MgAl2O4
T=950 °C T=135 min	0.381	0.398	0.986	AlN,MgO,MgAl2O4

APPENDIX C

In order to calculate XRD patterns, the crystallographic data and atom positions in the

unit cell must be known. The following tables show the crystal structure data of phases:

Table C-1: *crystal structure and atom positions of alumina*

		Al2O3			
Spacegrup		R-3 2/c			
Spacegroup Number		167			
Lattice Parameter		a	b	c	
		4.759(0)	4.759(0)	12.992(0)	
Angles		α	β	γ	
		90.00	90.00	120.00	
Atoms in Unit Cell		30			
Atoms					
Al			O		
Wyckoff position					
12c			**18e**		
x	y	z	x	y	z
0.0000	0.0000	0.8520	0.3060	0.0000	0.2500

Table C-2: *crystal structure and atom positions of aluminum nitride*

			AlN		
Spacegrup			P6_3 mc		
Spacegroup Number			186		
Lattice Parameter			a	b	c
			3.1100(0)	3.1100(0)	4.9800(0)
Angles			α	β	γ
			90.00	90.00	120.00
Atoms in Unit Cell			4		
Atoms					
Al			N		
Wyckoff position					
2b			2b		
x	y	z	x	y	z
0.3333	0.6667	1.0000	0.3333	0.6667	0.3821

Table C-3: *crystal structure and atom positions of magnesia*

	MgO		
Spacegrup	F4/m-3 2/m		
Spacegroup Number	225		
Lattice Parameter	a	b	c
	4.2109(0)	4.2109(0)	4.2109(0)
Angles	α	β	γ
	90.00	90.00	90.00
Atoms in Unit Cell	8		
Atoms			
Mg	O		
Wyckoff position			
4a			4b

x	y	z	x	y	z
0.0000	0.0000	0.0000	0.5000	0.5000	0.5000

Table C-4: *crystal structure and atom positions of spinel*

	MgAl$_2$O$_4$		
Spacegrup	F4_1/d-3 2/m		
Spacegroup Number	227		
Lattice Parameter	a	b	c
	8.0750(0)	830750(0)	8.0750(0)
Angles	α	β	γ
	90.00	90.00	90.00
Atoms in Unit Cell	56		

Atoms								
Mg			Al			O		
Wyckoff position								
8a			16d			32e		
X	Y	Z	X	Y	Z	X	Y	Z
0.00	0.00	0.00	0.625	0.625	0.625	0.361	0.361	0.361